# The diversity of CM carbonaceous chondrite parent bodies explored using Lewis Cliff 85311

Available online at www.sciencedirect.com

ScienceDirect

Geochimica et Cosmochimica Acta 264 (2019) 224–244

Geochimica et Cosmochimica Acta

www.elsevier.com/locate/gca

# The diversity of CM carbonaceous chondrite parent bodies explored using Lewis Cliff 85311

Martin R. Lee [a,*], Benjamin E. Cohen [a], Ashley J. King [b], Richard C. Greenwood [c]

[a] School of Geographical and Earth Sciences, University of Glasgow, G12 8QQ, UK
[b] Department of Earth Science, Natural History Museum (London), Cromwell Road, London SW7 5BD, UK
[c] Planetary and Space Sciences, Open University, Walton Hall, Milton Keynes MK7 6AA, UK

Received 17 May 2019; accepted in revised form 14 July 2019; available online 23 July 2019

**Abstract**

Lewis Cliff (LEW) 85311 is classified as a Mighei-like (CM) carbonaceous chondrite, yet it has some unusual properties that highlight an unrealised diversity within the CMs, and also questions how many parent bodies are sampled by the group. This meteorite is composed of rimmed chondrules, chondrule fragments and refractory inclusions that are set in a fine-grained phyllosilicate-rich matrix. The chondrules are of a similar size to those in the CMs, and have narrow fine-grained rims. LEW 85311 has been mildly aqueously altered, as evidenced by the preservation of melilite and kamacite, and X-ray diffraction results showing a low phyllosilicate fraction and a high ratio of cronstedtite to Fe, Mg serpentine. The chemical composition of LEW 85311 matrix, fine-grained rims, tochilinite and P-rich sulphides is similar to mildly aqueously altered CMs. LEW 85311 is enriched in refractory elements and REEs such that its CI-normalised profile falls between the CMs and CVs, and its oxygen isotopic composition plots in the CV-CK-CO field. Other distinctive properties of this meteorite include the presence of abundant refractory inclusions, and hundreds of micrometer size objects composed of needle-fibre calcite. LEW 85311 could come from part of a single CM parent body that was unusually rich in refractory inclusions, but more likely samples a different parent body to most other members of the group that accreted a subtly different mixture of materials. The mineralogical and geochemical evolution of LEW 85311 during subsequent aqueous alteration was similar to other CMs and was arrested at an early stage, corresponding to a petrologic subtype of CM2.7, probably due to an unusually low proportion of accreted ice. The CM carbonaceous chondrites sample multiple parent bodies whose similar size and inventory of accreted materials, including radiogenic isotopes, led to a comparable post-accretionary evolution.


*Keywords:* Carbonaceous chondrite; parent body; oxygen isotopes; refractory inclusions; aqueous alteration

## 1. INTRODUCTION

The Mighei-like (CM) meteorites are primitive rocks that are rich in water and organic molecules and so are particularly important for understanding the potential for volatiles to have been delivered to the terrestrial planets by asteroids and comets (Alexander et al., 2012). CMs have spectroscopic affinities to the ~13% of classified asteroids that belong to the C-complex (DeMeo et al., 2009; Cloutis et al., 2011). The C-complex includes B, C, Cb, Cg, Cgh and Ch types, which are most common in the outer part of the main asteroid belt, and ~60% of them have spectroscopic signatures of hydrated silicates (Burbine, 2017). Current exploration of the near-Earth asteroids Bennu and Ryugu will greatly enhance our understanding of the links between carbonaceous chondrites and their parent bodies. Bennu is a B-type asteroid with a hydrated surface and has spectroscopic affinities to the highly aqueously

* Corresponding author.
*E-mail address:* Martin.Lee@Glasgow.ac.uk (M.R. Lee).

https://doi.org/10.1016/j.gca.2019.07.027
0016-7037/

altered CMs (Hamilton et al., 2019). Reflectance spectra of the C-type asteroid Ryugu reveal abundant hydroxyl-bearing minerals, and its closest analogues are the thermally/shock metamorphosed carbonaceous chondrites (Kitazato et al., 2019).

The nature and diversity of hydrated carbonaceous asteroids can also be explored by investigating variability within the CM meteorites as they are the most abundant group of carbonaceous chondrites. The CMs are typically composed of chondrules (~20 vol.%) and refractory inclusions (~5 vol.%) that are supported in a fine-grained matrix (~70 vol.%) (Weisberg et al., 2006). The chondrules and refractory inclusions characteristically have fine-grained rims (FGRs) (e.g., Metzler et al., 1992). All of the CMs have undergone parent body aqueous alteration (e.g., McSween, 1979a,b; Bunch and Chang, 1980; Barber, 1981). Phyllosilicates are the most abundant alteration product; they comprise 56–91 vol.% of the bulk rock (Howard et al., 2009, 2011, 2015; King et al., 2017) and are the main constituent of the matrices and FGRs. The most reactive of the original components, namely mesostasis glass in chondrules, melilite in refractory inclusions, and amorphous material in the matrix and FGRs, is preserved only in the most mildly altered CMs including Yamato (Y) 791198, Paris, Elephant Morraine (EET) 96029 and Jbilet Winselwan (Chizmadia and Brearley, 2008; Hewins et al., 2014; Rubin, 2015; Lee et al., 2016; King et al., 2019). The variability in the degree of aqueous alteration of the CMs must reflect differences between parent body regions in properties such as: (i) the initial ratio of anhydrous material (silicate, sulphide, metal) to water ice; (ii) proximity to regions of fluid flow (e.g., Palguta et al., 2010); (iii) the duration and/or temperature of alteration, which may in turn relate to depth in the body or the intensity/frequency of collisional processing (Rubin, 2012; Hanna et al., 2015). Members of the CM group could therefore have been sourced from different locations within a single parent body (e.g., the more altered CMs could have come from deeper in the parent body where temperatures were higher), or from two or more bodies that may have evolved in contrasting ways (controlled for example by their size, initial abundance of short-lived radionuclides or shock history).

Here we ask whether Lewis Cliff (LEW) 85311 can help to define the extent of heterogeneity of a single CM parent body, or provide new insights into the diversity of multiple hydrated carbonaceous chondrite parent bodies with CM-affinities. This meteorite has come to our attention because its bulk chemical composition suggests that it is a mildly aqueously altered CM (Xiao and Lipschutz, 1992; Alexander et al., 2013; Friedrich et al., 2018) whereas its bulk oxygen isotopic composition indicates that it is an anomalous carbonaceous chondrite (Clayton and Mayeda, 1999; Choe et al., 2010). We have therefore undertaken a petrographic, mineralogical, chemical and isotopic study of LEW 85311 with a focus on understanding the variety of materials that were accreted, and the nature of subsequent parent body processing. In tandem, we have analysed a suite of CMs in order to provide a benchmark for interpreting the results from LEW 85311.

## 2. MATERIALS AND METHODS

### 2.1. Meteorites studied

LEW 85311 was recovered by ANSMET in 1985, and is paired with LEW 85306, 85309 and 85312. It has a mass of 199.5 g, a weathering grade of Be and a shock stage of S1 (Scott et al., 1992; Grossman, 1994). LEW 85311 is classified as CM2 (*Antarctic Meteorite Newsletter* 2008, vol. 31). This study used three polished thin sections (LEW 85311,31 (~11 × 14 mm); LEW 85311,39 (~11 × 8 mm); LEW 85311,90 (~9 × 7 mm)) and a 2.921 g chip (LEW 85311,84). Fifteen CMs were also studied for comparison with LEW 85311. They are listed in Table 1, along with their petrologic type (i.e., degree of aqueous alteration) relative to three classification schemes. None of these CMs have undergone significant post-hydration heating (Alexander et al., 2013).

### 2.2. Scanning and transmission electron microscopy

Each thin section was coated with a thin layer of carbon then studied using a Zeiss Sigma field-emission scanning electron microscope (FEG-SEM) operated at high vacuum. The Sigma is equipped with an Oxford Instruments XMax silicon-drift energy-dispersive X-ray spectrometer (EDX) operated through Oxford Instruments AZtec/INCA software. Backscattered electron (BSE) images were obtained at 20 kV/~1 nA. Point counting was undertaken by traversing the thin sections using the stepwise stage movement function. The apparent diameters of chondrules and refractory inclusions were determined from BSE images. The apparent diameter of these objects is expressed as: (long axis + short axis)/2, where the short axis is the diameter of the chondrule/refractory inclusion taken mid way along its length. Apparent FGR thickness was calculated as: (chondrule apparent diameter with FGR - chondrule apparent diameter without FGR)/2. X-ray maps were acquired from entire thin sections and from individual objects at 20 kV/3 nA and a 1024 × 768 pixel resolution, with the spectra being processed using AZtec. Quantitative chemical analyses were acquired using the Sigma operated at 20 kV/2 nA, with beam currents monitored using a Faraday cup. Spectra were acquired for 60 seconds, and quantified using INCA software. Calibration used the following mineral standards, with typical detection limits (wt.% element) in parentheses: Na, jadeite (0.10); Mg, periclase (0.06); Al, corundum (0.10); Si, diopside (0.11); P, apatite (0.12), S, pyrite (0.10), Cl, tugtupite (0.12), K, orthoclase feldspar (0.12); Ca, wollastonite (0.10); Ti, rutile (0.18); Cr, chromite (0.22); Mn, rhodonite (0.25); Fe, garnet (0.26); Ni, Ni metal (0.38). Co was not quantified owing to a peak overlap with Fe.

Electron-transparent foils for transmission electron microscopy (TEM) and scanning transmission electron microscopy (STEM) were cut and extracted from selected parts of the thin sections using a FEI duomill Focused Ion Beam (FIB) instrument operated using 30 kV $Ga^+$ ions and over a range of beam currents during the milling process (Lee et al., 2003). Foils were initially milled to a

Table 1
Meteorite samples studied.

| Meteorite | Fall or find/location/year | Weathering grade | Petrologic (sub)type | | |
|---|---|---|---|---|---|
| | | | Rubin[1] | Alexander[2] | Howard[3] |
| Allan Hills (ALH) 83100 | Find/Antarctica/1983 | Be | 2.1 | 1.1 | 1.2 |
| Allan Hills (ALH) 83102 | Find/Antarctica/1983 | B/Ce | 2.1 | 1.1 | 1.2 |
| Cold Bokkeveld | Fall/South Africa/1838 | n.a. | 2.2 | 1.3 | 1.4 |
| D'Angelo Bluff (DNG) 06004 | Find/Antarctica/2006 | B | – | 1.8 | 1.7 |
| Dominion Range (DOM) 08013 | Find/Antarctica/2008 | B/C | – | 1.8 | 1.5 |
| LaPaz Icefield (LAP) 02239 | Find/Antarctica/2002 | B | – | 1.7 | 1.4[7] |
| Lewis Cliff (LEW) 85311 | Find/Antarctica/1985 | Be | 2.6–2.7[4] | 1.9[6] | 1.7[7] |
| MacKay Glacier (MCY) 05230 | Find/Antarctica/2005 | B | – | 1.8 | – |
| Meteorite Hills (MET) 01075 | Find/Antarctica/2001 | B | – | 1.5 | 1.3[8] |
| Mighei | Fall/Ukraine/1889 | n.a. | – | 1.6 | 1.4 |
| Murchison | Fall/Australia/1969 | n.a. | 2.5 | 1.6 | 1.5 |
| Murray | Fall/USA/1950 | n.a. | 2.4/2.5 | 1.5 | 1.5 |
| Nogoya | Fall/Argentina/1879 | n.a. | 2.2 | 1.1/1.6 | 1.2/1.4 |
| Queen Alexandra Range (QUE) 97990 | Find/Antarctica/1997 | Be | 2.6 | 1.7 | 1.6 |
| Queen Alexandra Range (QUE) 99355 | Find/Antarctica/1999 | B | 2.3 | 1.5 | – |
| Scott Glacier (SCO) 06043 | Find/Antarctica/2006 | B/Ce | 2.0[5] | 1.1/1.2 | 1.2 |

– not determined.
n.a. not applicable as it is a fall.
[1] Rubin et al. (2007).
[2] Alexander et al. (2013).
[3] Howard et al. (2009, 2011, 2015).
[4] Tentative classification (Choe et al. 2010).
[5] This meteorite is a CM1, and so equivalent to CM2.0 of Rubin et al. (2007).
[6] LEW85312 is paired with LEW 85311 and has petrologic type of 1.8.
[7] Measured for the present study.
[8] Lee et al. (2019a,b).

thickness of ~1 μm, then extracted using an in-situ micromanipulator and welded to the tines of a Cu grid using ion and electron beam deposited platinum. They were then milled to ~100 nm thickness and loaded into a double-tilt goniometer holder. Bright-field images and selected area electron diffraction (SAED) patterns were acquired using a FEI T20 TEM operated at 200 kV. High angle annular dark-field (HAADF) imaging and quantitative X-ray microanalysis used a JEOL ARM200F field-emission STEM operated at 200 keV. For the analyses the ARM was operated with a 182 pA probe current and spectra were acquired and processed using a Bruker 60 $mm^2$ SDDEDX spectrometer operating Esprit V2.2 software.

### 2.3. X-ray diffraction (XRD)

A ~85 mg chip of LEW 85311 was powdered using an agate mortar and pestle. Approximately 50 mg of the powder was then packed into an aluminium sample well and analysed using an INEL X-ray diffractometer (XRD) with a curved 120° position sensitive detector (PSD) at the Natural History Museum (NHM), London. Copper $K_{\alpha 1}$ radiation was selected and XRD patterns were collected from the meteorite sample for 16 hours, throughout which time it was rotated. Standards of all minerals identified (except tochilinite as we do not have a pure sample) in LEW 85311 were analysed for 30 min. Modal mineral abundances were determined using a profile-stripping method that has now been applied to >30 CM chondrites (e.g. Howard et al. 2015; King et al. 2017). Briefly, the XRD pattern of each mineral standard was scaled to the same measurement time as the meteorites (i.e., ×32 for 16 h). The standard pattern was then reduced in intensity until it matched the intensity in the meteorite patterns, at which point it was subtracted to leave a residual pattern. After subtracting all of the mineral standards there were zero counts in the residual, and the fit factors were corrected for relative differences in X-ray absorption to give their final volume fractions in LEW 85311.

### 2.4. Oxygen isotopic analysis

Oxygen isotopic analysis of LEW 85311 was undertaken by infrared laser fluorination at the Open University (Miller et al., 1999; Greenwood et al., 2017). When analysing predominantly anhydrous samples it is normal procedure to reduce the system blank by flushing the chamber with at least two aliquots of $BrF_5$, each held in the chamber for 20 min. However, for samples that contain a significant proportion of phyllosilicates, such as CMs, this protocol can be problematic as it may result in preferential reduction in the hydrated silicate fraction prior to the high temperature fluorination step. This is because phyllosilicates can react with $BrF_5$ at low temperature during this blank reduction procedure. To minimise this problem, LEW 85311 was run in "single shot" mode, with only one standard and one aliquot of LEW 85311 loaded at a time (Schrader et al., 2014). This involved a four-stage procedure: (1) a 5 min

$BrF_5$ measured blank was run prior to the analysis of LEW 85311, (2) a single ~2 mg aliquot of the meteorite was then analysed, (3) a second 2 min measured blank was conducted after this analysis and finally (4) the isotopic composition of the internal obsidian standard was then measured. After fluorination, the $O_2$ gas released was purified by passing it through two cryogenic nitrogen traps and over a bed of heated KBr. The isotopic composition of the purified oxygen gas was then analysed using a Thermo Fisher MAT 253 dual inlet mass spectrometer (mass resolving power ~200). Interference at m/z = 33 by $NF^+$ was monitored by performing scans for $NF_2^+$ on the sample gas following initial analysis. As $NF_2^+$ was below interference levels no further sample treatment was required.

Analytical precision (2σ) for the Open University system, based on replicate analyses of an internal obsidian standard, is ±0.05‰ for $\delta^{17}O$; ±0.09‰ for $\delta^{18}O$; ±0.02‰ for $\Delta^{17}O$ (2σ) (Starkey et al., 2016). Oxygen isotopic analysis for LEW 85311 are reported in standard δ notation, where $\delta^{18}O$ has been calculated as: $\delta^{18}O = [(^{18}O/^{16}O)_{sample}/(^{18}O/^{16}O)_{ref} - 1] \times 1000$ (‰) and similarly for $\delta^{17}O$ using the $^{17}O$ /$^{16}O$ ratio, the reference being Vienna Standard Mean Ocean Water (VSMOW). For the purposes of comparison with the results of Clayton and Mayeda (1999) $\Delta^{17}O$, which represents the deviation from the terrestrial fractionation line, has been calculated as: $\Delta^{17}O = \delta^{17}O - 0.52 \times \delta^{18}O$.

## 3. RESULTS

### 3.1. Bulk chemical and oxygen isotopic composition

Bulk samples of LEW 85311 and LEW 85312 have been chemically and isotopically analysed by Xiao and Lipschutz (1992), Choe et al. (2010), Alexander et al. (2012, 2013), Friedrich et al. (2018) and Mahan et al. (2018) (Supplementary Table A1). These datasets can be used to assess the affinity of LEW 85311 to other carbonaceous chondrite groups. The ratio of elements with different volatilities is taxonomically indicative, namely highly volatile (Zn) to moderately volatile (Mn) and refractory (Sc) (i.e., Sc/Mn and Zn/Mn) (Kallemeyn and Wasson, 1981; Friedrich et al., 2018) (Table 2). Using these ratios, Friedrich et al. (2018) place LEW 85311 within the range of 15 CMs that they had also analysed. However, data in Choe et al. (2010) and average Sc/Mn and Zn/Mn values from all of the previous studies plot slightly outside of this range, although still much closer to the CMs than other carbonaceous chondrite groups (Table 2). The CI-normalised elemental composition of LEW 85311 is comparable to Paris (here chosen as representative of a mildly aqueously altered CM) for elements with 50% condensation temperatures less than Nb (1559 K), whereas the more refractory elements and most REEs plot between Paris and the CV carbonaceous chondrites (Fig. 1, Supplementary Table A1).

The bulk oxygen isotopic composition of LEW 85311 was originally determined by Clayton and Mayeda (1999). They classified LEW 85311 as an ungrouped carbonaceous chondrite (C2) on the basis of its "exceptional" oxygen isotope composition, but noted that "volatile and labile trace elements in LEW 85311 are typical of CM2 chondrites (Xiao and Lipschutz, 1992)." In addition, the matrix separate of LEW 85311 that was analyzed by Clayton and Mayeda (1999) plots within the CM2 field (Fig. 2), providing evidence for a possible genetic link between LEW 85311 and the CMs. The bulk oxygen isotope analysis of LEW 85311 undertaken for the present study is richer in $^{16}O$ than that of Clayton and Mayeda (1999) and plots well inside the CV-CK-CO field (Greenwood et al., 2010; Alexander et al., 2018) (Fig. 2, Table 3).

### 3.2. XRD modal mineralogy

The XRD pattern and modal mineralogy of LEW 85311,84 is comparable to the least altered CMs (Table 4). It has a phyllosilicate fraction (PSF) of 0.67 (where PSF = total phyllosilicate/(total anhydrous silicate + total phyllosilicate)), corresponding to type 1.7 on the classification scheme of Howard et al. (2009, 2011, 2015). LEW 85311 stands out from those CMs whose modal mineralogy has been quantified using XRD by virtue of its relatively high abundance of Fe,Ni metal (0.3 vol.%), scarcity of sulphide (0.5 vol.%), absence of calcite, low PSF and high ratio of cronstedtite to Fe, Mg serpentine (Fig. 3).

### 3.3. Petrography and mineralogy

The constituents of LEW 85311,39 as determined by SEM point counting are (in vol.%, n = 848): matrix (39.9); FGRs (30.7); chondrules, chondrule fragments and refractory inclusions (29.2) (Fig. 4). Calcite-rich objects comprise 0.2 vol.%, in agreement with the low abundance

Table 2
Mn, Sc and Zn element composition of LEW 85311 compared to the CMs.

| | LEW 85311[1] | LEW 85311[2] | LEW 85311[3] | LEW 85312[4] | Average[1–4] | CMs (n = 15)[3] |
|---|---|---|---|---|---|---|
| Sc (μg/g) | n.a. | 7.6 | 7.36 | n.a. | 7.5 | 6.99–8.96 |
| Mn (μg/g) | n.a. | 1880 | 1690 | n.a. | 1785 | 1460–1870 |
| Zn (μg/g) | 179 | 151 | 203 | 155 ± 17 | 172 | 171–242 |
| Sc/Mn × 1000 (at) | – | 4.9 | 5.3 | – | 5.1 | 5.2–6.5 |
| Zn/Mn × 100 (at) | – | 6.8 | 10.1 | – | 8.1 | 8.6–11.1 |

n.a. – not analysed.
[1] Xiao and Lipschutz (1992).
[2] Choe et al. (2010).
[3] Friedrich et al. (2018).
[4] Mahan et al. (2018).

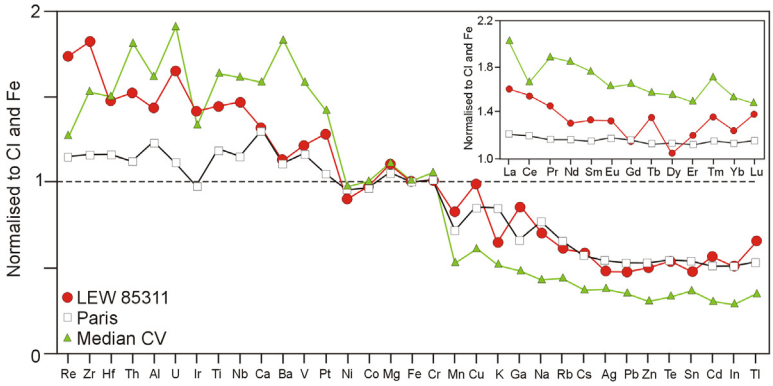


Fig. 1. The chemical composition of LEW 85311 normalised to CI (Ivuna) and Fe. The main graph elements are arranged in order of 50% condensation temperature (Lodders, 2003), decreasing to the right. The inset shows REE in Z order, also normalized to CI and Fe. Data from Paris (CM2.7) and the median of three CVs are plotted for comparison. Ivuna, Paris and the CV data are from Braukmüller et al. (2018) (note that Paris contains lithologies with different degrees of aqueous alteration, but the relationship of the sample analysed to these lithologies is unknown). LEW 85311 data are from Xiao and Lipschutz (1992), Choe et al. (2010), Friedrich et al. (2018) and Mahan et al. (2018) (Supplementary Table A1). An average value has been used where the same element was measured in two or more these studies.

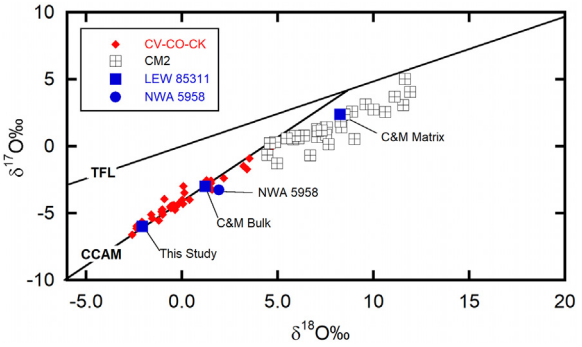


Fig. 2. Bulk oxygen isotopic composition of a subsample of LEW 85311,84 analysed in the present study compared to the data of Clayton and Mayeda (1999) (C&M). NWA 5958 (C2-ung) is also plotted (Jacquet et al., 2016). TFL – Terrestrial Fractionation Line. CCAM – Carbonaceous Chondrite Anhydrous Mineral. CV-CO-CK data from Greenwood et al. (2010) and Alexander et al. (2018).

Table 3
Oxygen isotopic composition of LEW 85311 and NWA 5958 (C2-ung).

| | LEW 85311 | | NWA 5958[2] |
|---|---|---|---|
| | The present study | Clayton and Mayeda[1] | |
| $\delta^{17}O$ (‰) | −5.98 | −2.98 | −3.25 |
| $\delta^{18}O$ (‰) | −2.07 | 1.21 | 1.92 |
| $\Delta^{17}O$ (‰) | −4.90 | −3.61 | −4.26 |

[1] Clayton and Mayeda (1999, Table 5).
[2] Mean of 3 analyses (Jacquet et al., 2016).

of this mineral as revealed by XRD. Table 5 lists point counting results from eight CMs for comparison.

### 3.3.1. Chondrules and chondrule fragments

A previous study of LEW 85311 found that it contains barred olivine (BO), porphyritic olivine (PO), porphyritic olivine–pyroxene (POP) and porphyritic pyroxene (PP) chondrules with an average apparent diameter of 190 μm (n = 100) (Choe et al., 2010) (Fig. 5). The 72 chondrules and chondrule fragments measured for the present study have an approximately log-normal distribution (Supplementary Fig. A1) with an average apparent diameter of 213 ± 153 μm. Chondrule fragments comprise one or several grains of olivine, pyroxene and/or Fe,Ni metal. Both intact and fragmented chondrules have FGRs. Fayalitic olivine in type II chondrules is very similar in composition to olivine in type II chondrules from Paris (CM) and Acfer 094 (C2-ung) (Supplementary Table A2). Olivine and pyroxene grains in intact chondrules are typically pristine, whereas in a few cases grains of fayalitic olivine within chondrule fragments have been partially replaced by phyllosilicates along their contact with the enclosing FGR (Fig. 5e and f). No chondrule mesostasis glass has been preserved, and in its place are pores, porous arrays of pyroxene crystallites or phyllosilicates (Fig. 5b). Chondrules can also contain rounded pores tens of micrometres in diameter (Fig. 5c).

Table 4
Modal mineralogy of LEW 85311,84 (vol.%).

| | |
|---|---|
| Cronstedtite | 37.8 |
| Mg-serpentine | 27.0 |
| Olivine | 21.4 |
| Enstatite | 10.1 |
| Sulphate | 1.7 |
| Magnetite | 1.2 |
| Fe-sulphide | 0.5 |
| Metal | 0.3 |
| Carbonate | n.d. |
| Phyllosilicate fraction (PSF) | 0.67 |
| Cronstedtite/Mg-serpentine | 1.40 |
| Petrologic type | 1.7 |

Determined by XRD.
n.d. – not detected.

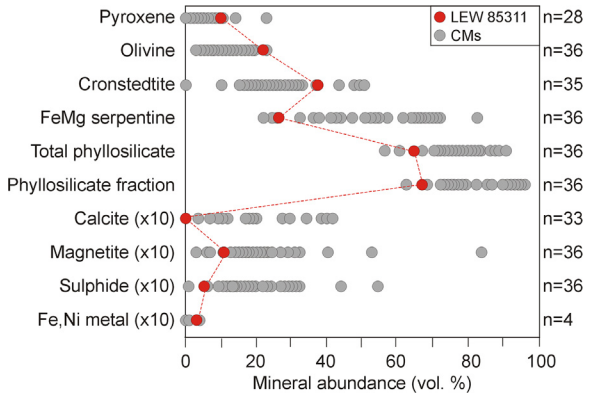


Fig. 3. The modal mineralogy of LEW 85311, as determined by XRD, compared to 36 CMs that have been analysed previously (Howard et al., 2009, 2011, 2015; King et al. 2017). The number of CMs with an above zero abundance of each mineral is indicated on the right hand side. Sulphates have not been included as they may be products of terrestrial weathering (Lee, 1993).

Many type I chondrules contain 'nuggets' of kamacite, which have an average composition of $Fe_{94.3}Ni_{5.2}Cr_{0.4}$ (11 analyses from five chondrules) (Fig. 5a). These kamacite grains have been partially or near-completely altered, and two compositionally and petrographically distinct types of alteration products are recognized: (i) Fe-rich/S-rich, which form a narrow rim to kamacite grains and also penetrate into their interior; (ii) Fe-rich/S-poor, which occur as a concentrically laminated mantle and veins extending from the mantle into the FGR (Fig. 6). The Fe-rich/S-rich material is dominated by Fe, Ni and S, and gives low analytical totals (Table 6). It is compositionally comparable to tochilinite that has formed by the alteration of kamacite in CM carbonaceous chondrites (Table 7) (Tomeoka and Buseck, 1985; Palmer and Lauretta, 2011). LEW 85311 tochilinite is closer in composition to tochilinite in the mildly altered CMs than in the more highly altered meteorites (Table 7). The Fe-rich/S-poor mantles yield low analytical totals (~79 wt.%) suggesting significant concentrations of unanalyzed $OH/H_2O$ (although other elements such as carbon, and porosity, can also contribute to the low totals) (Table 6). The detection of Cl suggests that akaganéite (β-FeOOH) is present. Akaganéite is a common weathering product of Antarctic iron meteorites and ordinary chondrites (Buchwald and Clarke, 1989) where it has the following compositional range (wt.%): Fe (39–60), Ni (0.5–19, with 3–5 being typical); Cl (0.3–5.4); S (0–2). Most analyses of LEW 85311 Fe-rich/S-poor mantles are within the range of Antarctic akaganéite (wt.%): Fe (38–54), Ni

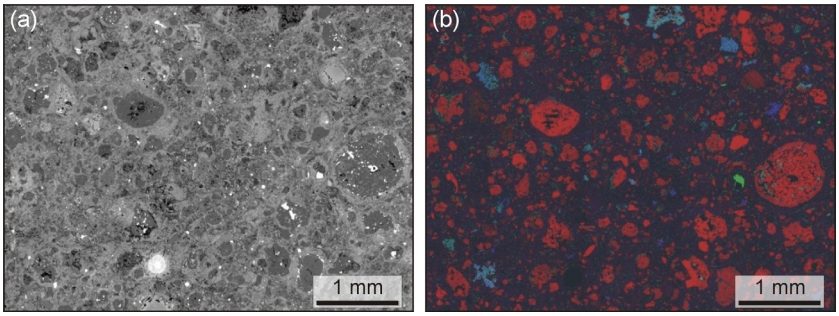


Fig. 4. BSE image (a) and multi-element X-ray map (Mg red, Al blue, Ca green) (b) of LEW 85311,90. The colour coding of (b) renders type I chondrules red, refractory inclusions light blue, calcite green, and the matrix and FGRs dark red. (For interpretation of the references to color in this figure legend, the reader is referred to the web version of this article.)

Table 5
Abundance (vol.%) of the three main constituents of LEW 85311 compared to eight CMs.

| | Objects | FGRs | Matrix[1] | Matrix/FGR | n | Petrologic type[2] |
|---|---|---|---|---|---|---|
| LEW 85311 | 29.4 | 30.7 | 39.9 | 1.3 | 848 | 1.9 |
| DNG 06004 | 33.7 | 13.9 | 52.4 | 3.8 | 700 | 1.8 |
| DOM 08013 | 37.0 | 23.5 | 39.6 | 1.7 | 230 | 1.8 |
| MCY 05230 | 30.0 | 23.3 | 46.7 | 2.0 | 180 | 1.8 |
| QUE 97990 | 36.1 | 18.2 | 45.7 | 2.5 | 269 | 1.7 |
| LAP 02239 | 29.3 | 14.5 | 56.1 | 3.9 | 399 | 1.7 |
| MET 01075 | 14.6 | 6.5 | 78.9 | 12.1 | 403 | 1.5 |
| QUE 99355 | 20.2 | 9.9 | 70.0 | 7.1 | 233 | 1.5 |
| Cold Bokkeveld | 13.5 | 4.0 | 82.5 | 20.6 | 252 | 1.3 |

Determined by SEM point counting.
Objects are chondrules, chondrule fragments and refractory inclusions.
n – number of points counted.
[1] Includes calcite grains.
[2] Alexander et al. (2013).

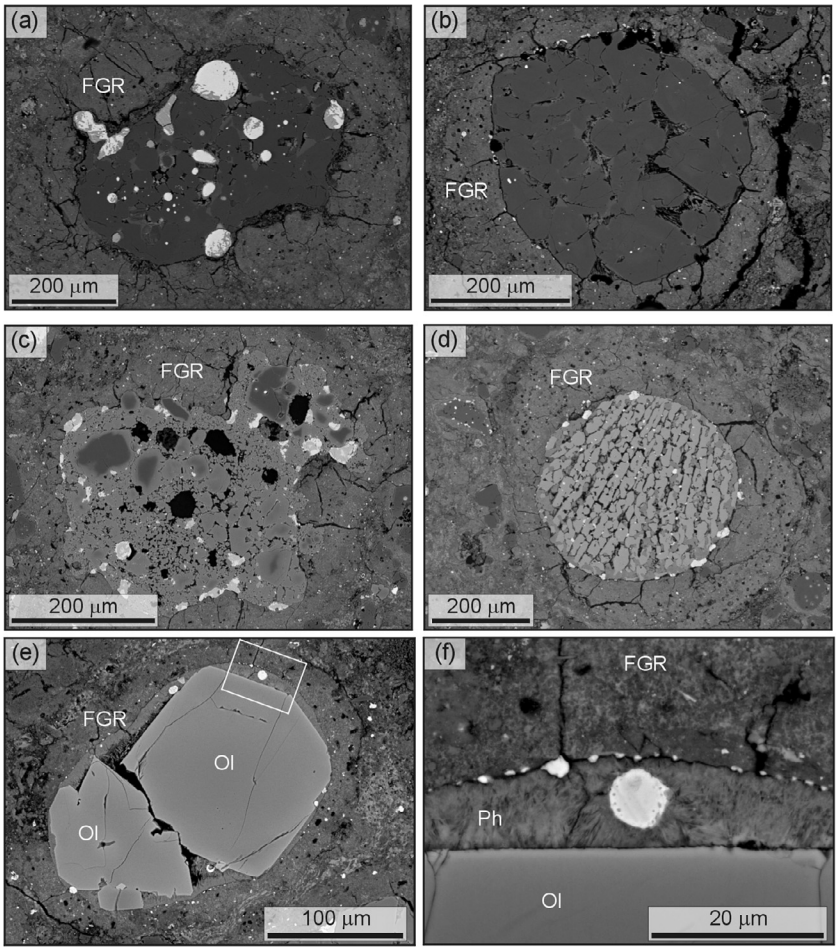


Fig. 5. BSE images of chondrules and chondrule fragments, and their enclosing radially fractured and micropore-rich FGRs. (a) POP chondrule in LEW 85311,31. Between the grains forsterite and enstatite (mid-grey) are small crystals of Ca-rich pyroxene (light grey; $En_{54}Wo_{45}Fs_1$). Nodules of kamacite (white) have been partially replaced by tochilinite (mid-grey). (b) POP chondrule in LEW 85311,31. Between the grains of forsterite and enstatite (mid-grey) are small crystals of Ca-rich pyroxene ($En_{55}Wo_{38}Fs_7$). Dissolution of the mesostasis has left micropores (black) with skeletal crystallites. (c) PO chondrule in LEW 85311,39. Some of the fayalitic olivine crystals are zoned and the chondrule has a significant internal porosity (black). (d) BO chondrule in LEW 85311,31. The small high-Z grains are Fe-sulphide. Between crystals of fayalitic olivine ($Fo_{25-56}$) are pyroxenes ($En_{38}Wo_1Fs_{61}$). (e) A grain of fayalitic olivine (Ol) in LEW 85311,39. (f) Detail of the contact of fayalitic olivine with its FGR (boxed area in (e)). The olivine has been partially replaced by phyllosilicate (Ph), probably cronstedtite. The high-Z (white) grains are Fe-sulphide.

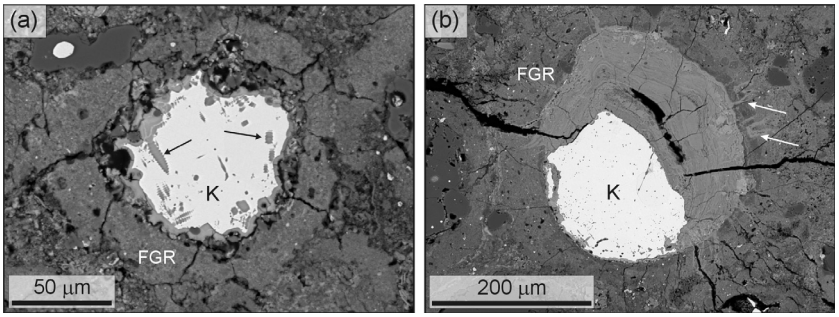


Fig. 6. BSE images of altered kamacite (K). (a) A grain in LEW 85311,31 enclosed by a FGR. Tochilinite (mid-grey) embays the outer edges of the kamacite grain and extends into its interior (arrowed). (b) A grain in LEW 85311,39 that has a thick and concentrically laminated mantle of Fe-rich/S-poor alteration products. Veins of the same material cross-cut the FGR (arrowed).

Table 6
Chemical composition (wt.%) of Fe- and S-bearing alteration products in LEW 85311 kamacite grains, calcite-rich objects and veins.

| | Fe-rich/S-poor | Fe-rich/S-rich | | |
|---|---|---|---|---|
| | Kamacite hosted | Kamacite hosted | Calcite-rich object hosted | Vein hosted |
| $SiO_2$ | 0.81 ± 0.61 | 3.03 ± 0.95 | 6.31 ± 0.50 | 5.53 ± 1.46 |
| $Al_2O_3$ | 0.12 ± 0.19 | 0.63 ± 0.15 | 0.83 ± 0.07 | 0.68 ± 0.20 |
| $Cr_2O_3$ | 1.33 ± 0.76 | 2.48 ± 1.43 | d.l. | 2.14 ± 0.33 |
| $Fe_2O_3$ | 65.35 ± 4.58 | 55.14 ± 3.11 | 58.92 ± 3.96 | 58.08 ± 1.83 |
| NiO | 4.45 ± 1.08 | 8.81 ± 0.85 | 6.30 ± 0.84 | 6.23 ± 0.02 |
| MgO | 0.70 ± 0.48 | 2.91 ± 0.44 | 2.19 ± 0.19 | 2.09 ± 0.21 |
| CaO | 0.26 ± 0.24 | 1.33 ± 0.24 | 1.19 ± 0.48 | 0.52 ± 0.17 |
| $Na_2O$ | 0.55 ± 0.25 | d.l. | 0.12 ± 0.10 | 0.50 ± 0.04 |
| $P_2O_5$ | 1.13 ± 0.43 | n.a. | 1.59 ± 0.58 | 2.06 ± 0.25 |
| Cl | 0.69 ± 0.53 | n.a. | 0.13 ± 0.10 | 0.24 ± 0.02 |
| S | 3.97 ± 2.39 | 16.88 ± 1.68 | 12.90 ± 0.96 | 8.17 ± 2.55 |
| Total | 79.37 | 91.56 | 90.55 | 86.25 |
| n | 26 | 5 | 15 | 2 |

K, Ti and Mn were sought, but below detection limits (d.l.).
n.a. – not analysed.
± One standard deviation.
Individual analyses provided in the supplementary data.

Table 7
Chemical composition (atomic) of Fe-rich/S-rich alteration products in kamacite grains from LEW 85311 and four CMs.

| | Mg/(Mg + Fe) | Ni/(Fe + S) | Petrologic type[3] |
|---|---|---|---|
| LEW 85311,31[1] | 0.10 ± 0.02 | 0.10 ± 0.01 | 1.9 |
| Murchison[2] | 0.12 | 0.12 | 1.6 |
| Murray[2] | 0.12 | 0.11 | 1.5 |
| Cold Bokkeveld[2] | 0.20 | 0.09 | 1.3 |
| Nogoya[2] | 0.18 | 0.05 | 1.1/1.6 |

± One standard deviation.
[1] Mean of five analyses of alteration products in two kamacite grains.
[2] Palmer and Lauretta (2011, Table 2).
[3] Alexander et al. (2013).

(2–6), Cl (<0.1–2), S (<0.1–12). The main difference to akaganéite in Buchwald and Clarke (1989) is a wider range of S, although only a few analyses have high S concentrations (Fig. 7). The low Cl values probably reflect an intergrowth of akaganéite with Cl-free goethite (Buchwald and Clarke, 1989).

### 3.3.2. Refractory inclusions

In order to assess the abundance, mineralogy and degree of preservation of refractory inclusions, those occurring in a 0.28 $cm^2$ area of LEW 85311,90 were studied in detail (Fig. 8a–c). This area contains 41 inclusions (146/$cm^2$). They have an apparent diameter of 20–402 μm (average 105 ± 88 μm) and an aspect ratio of 1.2–6.5 (average 2.5 ± 1.2). The mineralogy and structure of all inclusions occurring in a 0.08 $cm^2$ part of the mapped region was determined. This area contains 15 inclusions. Seven of them are dominated by spinel and pyroxene (Fig. 8a), four by spinel and perovskite (Fig. 8b), and each of the others contains one refractory mineral (spinel, perovskite, pyroxene, gehlenite; Fig. 8c). Most of the inclusions are porous and contain phyllosilicates (e.g., Fig. 8b); the gehlenite grain has been partially replaced by coarse grained phyllosilicate (Fig. 8c). Among the 15 inclusions are five morphological types (after Rubin 2007): five banded, three nodular, two simple, three simple distended and two complex distended.

In addition to occurring in LEW 85311,90, gehlenite is present in a refractory inclusion in LEW 85311,39, where it is accompanied by spinel, perovskite, pyroxene and Ca-carbonate (Fig. 8d and e). Its empirical formula is $Ca_{2.0}Al_{1.5}Mg_{0.2}Si_{1.2}O_7$ (average of two analyses). The presence of pores surrounding the gehlenite, and the occurrence of small relict gehlenite grains (Fig. 8e) suggests that it has survived partial dissolution. Melilite-bearing refractory inclusions were also described from LEW 85311 by Simon et al. (2005). They found two inclusions where melilite mantles hibonite, and this relationship was interpreted to show that the melilite formed earlier. Although most LEW 85311refractory inclusions are comparable in mineralogy and morphology to those in the CMs (Rubin et al., 2007), the LEW 85311,31 thin section contains a rare forsterite chondrule enclosing a simple spinel-perovskite refractory inclusion (Fig. 8f). Reaction of forsterite with spinel has formed a high-Z material that is rich in O, Al, Si, Ca and Ti (Fig. 8f).

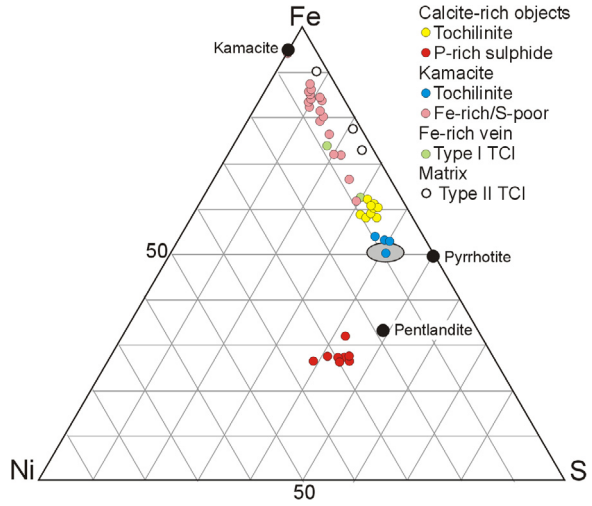


Fig. 7. The compositions (at.%) of Fe- and S-bearing phases hosted in LEW 85311 calcite-rich objects, kamacite grains, a Fe-rich vein and the matrix. All analyses of the material within the calcite objects, Fe-rich vein, kamacite nuggets and matrix (except P-rich sulphide) plot along a line $(Fe + S)_{90\text{-}95}Ni_{10\text{-}5}$. The grey oval delineates the compositional range of tochilinite after kamacite in CM chondrules (Palmer and Lauretta, 2011). LEW 85311 pentlandite and pyrrhotite data are from Kimura et al. (2011) whereas the composition of kamacite is from the present study.

### 3.3.3. Calcite-rich objects

Most LEW 85311 Ca-carbonate occurs as meshworks of needle-fibre crystals, which are present in all three thin sections and most abundant in LEW 85311,39. This Ca-carbonate occurs in two petrographic contexts: (i) small (10 s μm) patches within chondrules and chondrule fragments (Fig. 9a–e); (ii) the main constituent of relatively large (>~100 μm) rounded, irregular or elongate objects that have a FGR (Fig. 10). The needle-fibre crystals were identified as calcite by SAED. On average they are ~18 μm in length by 2 μm in width. Individual fibres are aggregates of ~1 μm wide acicular crystals (Fig. 9d and f). The fibres may be straight or curved, sometimes to such an extent that they are almost circular (Fig. 9d). Most fibres are oriented randomly relative to each other, although those at the edges of the meshworks may be aligned with their long axes roughly parallel to each other in a radiating or palisade structure (Fig. 9b). TEM shows that the fibres have a low defect density and no inclusions (Fig. 9f).

In almost all objects the needle-fibre calcite is associated with one or more Fe- and Cr-rich minerals (kamacite, Fe-sulphide, schreibersite, P-rich sulphide, eskolaite) (Figs. 9 and 10) (Supplementary Table A3). The kamacite grains are usually rimmed or cross-cut by Fe-rich/S-rich alteration products whose composition is similar to tochilinite after kamacite (Table 6). The average formula for the P-rich sulphides is $Fe_{2.0}Ni_{2.2}S_{3.2}P_{0.8}$ (normalized to Fe = 2; n = 9 analyses), which is similar to P-rich sulphides elsewhere in LEW 85311 that were analysed by Nazarov et al. (2009) (Table 8). Fe-sulphide, schreibersite and eskolaite crystals tend to be present at the margins of the meshworks, whereas the tochilinite and P-rich sulphide occur within them (Figs. 9a, b, e and 10).

### 3.3.4. Fe-rich veins

Two Fe-rich veins occur in LEW 85311,31 (Fig. 11). One is 500 μm in length by 15 μm in width and has a FGR (Fig. 11a). It contains grains of kamacite, Fe-sulphide and schreibersite in a matrix of a Fe-rich/S-rich material that is comparable in composition to tochilinite after kamacite in LEW 85311 chondrules (Table 5, Supplementary Table A3). The other vein is partly wrapped around a chondrule fragment and is composed solely of tochilinite and P-rich sulphide (Fig. 11b).

### 3.3.5. Matrix and FGRs

LEW 85311 matrix and FGRs yield low analytical totals that are consistent with a phyllosilicate-rich mineralogy (Supplementary Table A4). Both components plot within the 'serpentine field' of a ternary diagram, and specifically between end-member serpentine, and LEW 85311 cronstedtite and tochilinite-cronstedtite intergrowths (TCIs) (Fig. 12). The matrix and FGRs have a lower Mg/(Mg + Fe) than the bulk meteorite (Fig. 12). Comparison of LEW 85311 matrix and FGR compositions with 13 CMs also analysed for the present study show a comparable pattern of depletion and enrichment, with LEW 85311 being compositionally closest to those CMs that have been mildly aqueously altered (Supplementary Fig. A2). The MgO/FeO ratio of CM matrices is informative about CM parent body history as it increases with progressive aqueous alteration (McSween, 1987). The value for LEW 85311 (0.33) is lower than the CM2.7 meteorite Paris (0.39) (Supplementary Table A4).

The apparent thickness of FGRs on chondrules and chondrule fragments ranges from 15 to 101 μm (average 37 ± 25 μm, n = 72), and is positively correlated with their diameter ($R^2 = 0.73$, slope = 0.14) (Supplementary Fig. A3). FGRs have a sharp contact with the matrix and are distinguished from it by a lower Fe/Si ratio (Supplementary Table A4) and a finer and more homogeneous grain size (Fig. 13a). Despite being more compact than the matrix, FGRs characteristically contain fractures and micropores (Fig. 13b). Fractures are typically oriented normal to the outer edge of the host object and pinch out towards the matrix (Fig. 5). Micropores are an average of 6 μm in size and some have a negative crystal shape. They can occur throughout the FGR, but are usually more abundant closer to the matrix (Fig. 13b). TEM shows that the FGRs contain silicate and sulphide mineral grains of a range of sizes, between which are cylindrical TCI and serpentine crystals (Fig. 13c–f).

The matrix contains fine silicate and sulphide grains together with clumps of phyllosilicates and rare grains of Ca-carbonate (Fig. 14). Particles ~1 μm in size also occur in the matrix that are similar in size and shape to amorphous domains in Y-791198 (Chizmadia and Brearley, 2008) and GEMS grains in Paris (Leroux et al., 2015); they are thus likely to be composed of amorphous silicate, sulphide and metal (Fig. 14b). Locally developed petrofabrics are evidence for mild ductile compaction of the matrix (Fig. 11b). TEM and STEM images show that the matrix contains platy and entangled cylindrical crystals (Fig. 14c and d). The platy crystals have a chemical composition

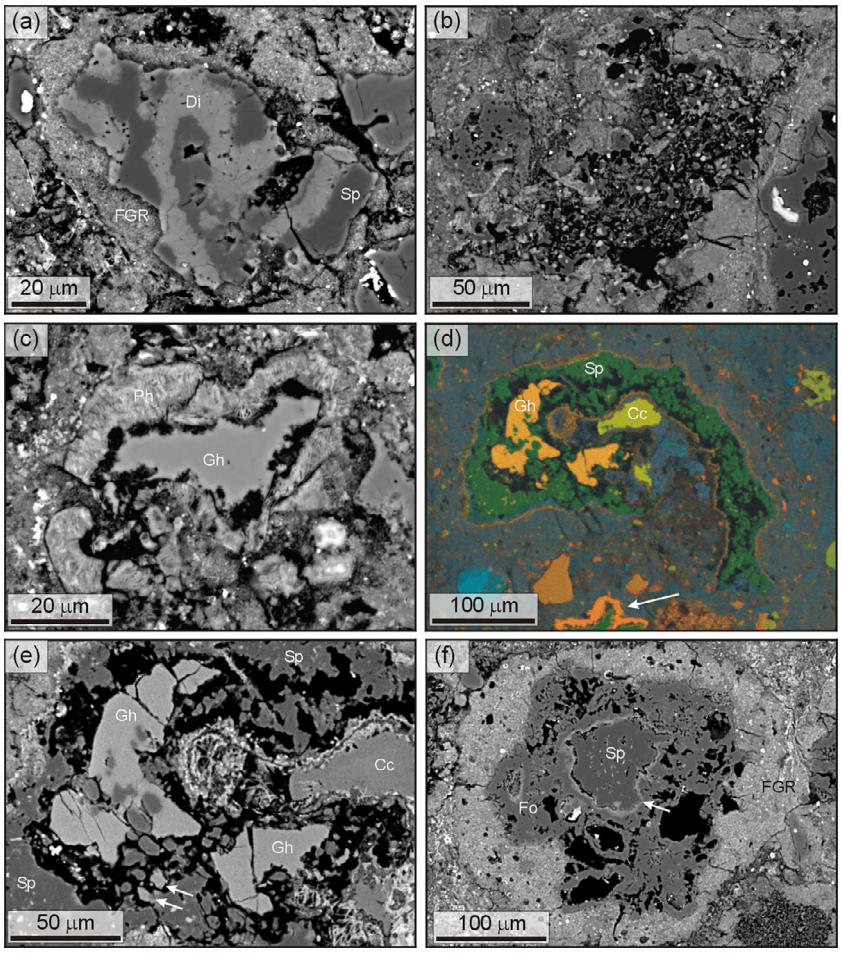


Fig. 8. Refractory inclusions, with morphology classification from Rubin (2007). (a)-(c) BSE images of inclusions from the area of LEW 85311,90 that was studied in detail. (a) A banded spinel (Sp)-diopside (Di) inclusion contained within a FGR. (b) A simple distended spinel-perovskite inclusion with a high microporosity (black). The edge of a chondrule is on the right hand side. (c) A simple inclusion comprising a crystal of gehlenite (Gh) whose edges have been etched and partly replaced by phyllosilicates (Ph). (d) X-ray map overlain on a BSE image of a simple inclusion in LEW 85311,39. The X-ray map has been coloured as follows: Mg light green, Si purple, Ca yellow, Fe light blue. This colouration highlights the main minerals: spinel (Sp, dark green), gehlenite (Gh, orange) and Ca-carbonate (Cc, light green). Part of another refractory inclusion is at the bottom of the image (arrowed). (e) BSE image of the left hand part of the inclusion in (d), highlighting the relationship of gehlenite to spinel and porosity (black). The arrows highlight two small grains of gehlenite. (f) Forsterite (Fo) chondrule in LEW 85311,31 that has a spinel (Sp)-perovskite refractory inclusion at its core. The selvage of high-Z material between the refractory inclusion and the forsterite (arrowed) is rich in Al, Si, Ca and Ti. (For interpretation of the references to color in this figure legend, the reader is referred to the web version of this article.)

close to that of cronstedtite in Paris (Table 9), and such a mineralogy is consistent with their ~0.7 nm lattice fringe spacing (Fig. 14d). The cylindrical crystals are intermediate in composition between cronstedtite and tochilinite (Table 9) and so are inferred to comprise an intergrowth of both minerals (i.e., type II TCI; Tomeoka and Buseck, 1985; Pignatelli et al., 2017). Although TCI has been identified within the matrix by TEM, the tens of micrometer size TCI clumps that characterize CM matrices are absent (as also noted by Choe et al., 2010).

## 4. DISCUSSION

Our petrographic, mineralogical, chemical and isotopic results show that LEW 85311 has both similarities and differences to the CMs. Below we describe the geological history of LEW 85311 and evaluate its affinity to the CM group through a discussion of the material that was accreted, and its subsequent mineralogical and geochemical evolution. We then consider the implications of these results for understanding the nature of its parent body, and specifically whether LEW 85311 comes from the same body(ies) as other members of the CM group, or is a piece of a different, and maybe previously unsampled, hydrated C-complex asteroid.

### 4.1. LEW 85311 geological history

#### *4.1.1. Accreted material*

The LEW 85311 parent body was formed by accretion of coarse-grained objects (chondrules, chondrule fragments, refractory inclusions), a fine-grained matrix, and

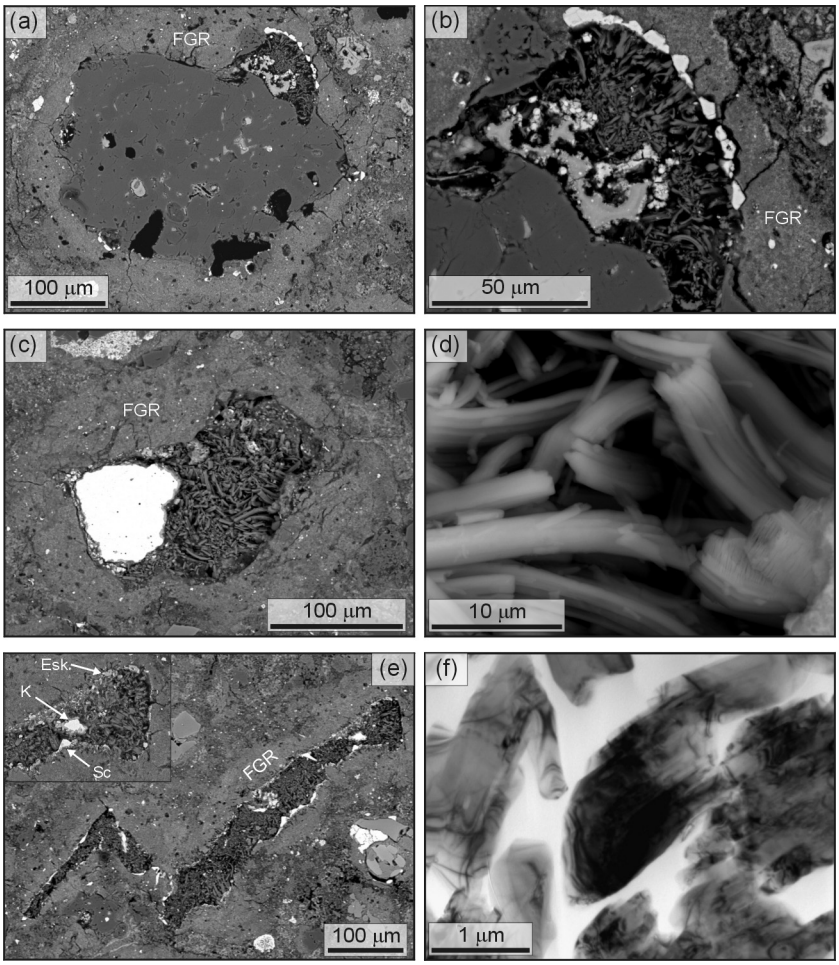


Fig. 9. Calcite-rich objects. (a)-(e) BSE images. (a) A POP chondrule in LEW 85311,31 that has a patch of needle-fibre calcite protruding from its upper right hand edge. The rounded black areas within the chondrule are pores. (b) The patch of calcite in (a), which comprises a porous meshwork of fibres. The white crystals that decorate the boundary between the patch and FGR are Fe-sulphide. The mid-grey material in the lower part of the patch is similar in chemical composition to tochilinite after kamacite. (c) An object in LEW 85311,90 that is composed of a large grain of kamacite (white) and a meshwork of calcite fibres. The object has a thick FGR. (d) The calcite fibres in (c), each of which is composed of a sheath of acicular crystals. (e) A shard-shaped calcite object in LEW 85311,39 with a FGR. The inset show that it contains small relict grains of kamacite (K) and its edges are lined by high-Z minerals including eskolaite (Esk) and schreibersite (Sc). (f) Bright-field TEM image of needle-fibre calcite from LEW 85311,39. Some of the fibres are aggregates of acicular crystals.

probably also water-rich ice. The origin of FGRs on the coarse-grained objects has been debated, with three processes being proposed: (i) accretion of dust within the solar nebula (e.g., Metzler et al., 1992); (ii) impact compaction of fine-grained matrix material around chondrules and other objects within the parent body (e.g., Trigo-Rodriguez et al., 2006); (iii) aqueous alteration of the host object (e.g., Sears et al., 1993). Clues to the origin of LEW 85311 FGRs come from their structure and composition. They have a sharp outer edge, which separates the compact and equigranular rim material from the more porous and mineralogically heterogeneous matrix. The FGRs also differ in chemical composition to the matrix (Supplementary Table A4), and their apparent thicknesses correlates well with the apparent diameter of their host objects (Supplementary Fig. A3). We propose that these properties are inconsistent with an origin by impact compaction, and best explained by accretion in the solar nebula. This conclusion agrees with results of an X-ray tomography study of Murchison FGRs by Hanna and Ketcham (2018). They also observed that the FGRs are compositionally uniform across different chondrule types, thus arguing against an origin by aqueous alteration of their more compositionally variable host objects. Chondrules, chondrule fragments and refractory inclusions therefore had FGRs when they were incorporated into the LEW 85311 parent body.

Relative to eight CMs analysed for the present study (Table 5), LEW 85311 contains the second lowest proportion of matrix and highest proportion of FGRs. It thus somewhat resembles the 'primary accretionary rock' lithology that characterises unbrecciated CMs (Metzler et al., 1992). The proportion of the meteorite that consists of chondrules, chondrule fragments and refractory inclusions (29.4%) is close to the CM average (26.8 vol.%) (Table 5).

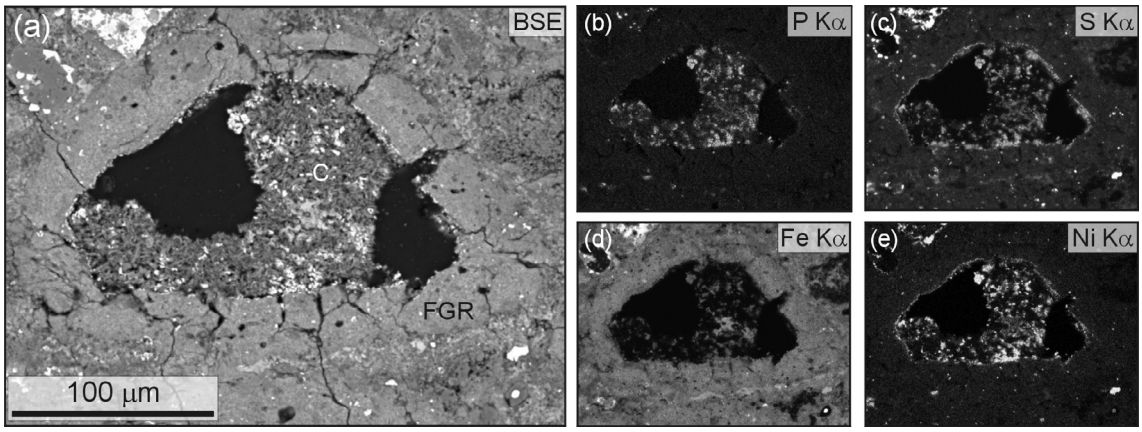


Fig. 10. BSE image (a) and X-ray element maps (b)–(e) of a calcite-rich object in LEW 85311,31 that is enclosed within a FGR. Calcite (C, mid grey) has been lost from two parts of the object (black), presumably during thin section preparation. The X-ray maps show that P, S, Fe and Ni are co-located as grains of P-rich sulphide that are intergrown with calcite.

Table 8
Chemical composition (atomic) of P-bearing sulphides in LEW 85311 and six CMs.

| | S/P | (Fe + Ni)/P | Fe/Ni | Petrologic type[3] |
|---|---|---|---|---|
| LEW 853111 | 3.78 ± 0.22 | 4.94 ± 0.30 | 0.94 ± 0.13 | 1.9 |
| LEW 853112 | 3.82 ± 0.80 | 5.10 ± 0.68 | 1.07 ± 0.08 | 1.9 |
| Murchison[2] | 3.36 ± 0.84 | 4.54 ± 0.80 | 0.93 ± 0.22 | 1.6 |
| Mighei[2] | 8.75 ± 3.00 | 9.37 ± 2.92 | 1.10 ± 0.20 | 1.6 |
| Murray[2] | 3.40 ± 0.52 | 4.55 ± 0.59 | 0.85 ± 0.11 | 1.5 |
| Cold Bokkeveld[2] | 9.10 ± 4.14 | 9.94 ± 4.06 | 1.20 ± 0.26 | 1.3 |
| Nogoya[2] | 12.40 ± 6.14 | 13.20 ± 6.01 | 1.21 ± 0.27 | 1.1/1.6 |
| ALH 83100[2] | 24.83 ± 5.88 | 25.17 ± 5.83 | 1.81 ± 0.32 | 1.1 |

± One standard deviation.
Individual analyses for LEW 85311 provided in the supplementary data.
[1]The present study. Ratios calculated from eight analyses of seven grains in LEW 85311,31 and one analysis of one grain in LEW 85311,90.
[2] Nazarov et al. (2009).
[3] Alexander et al. (2013).

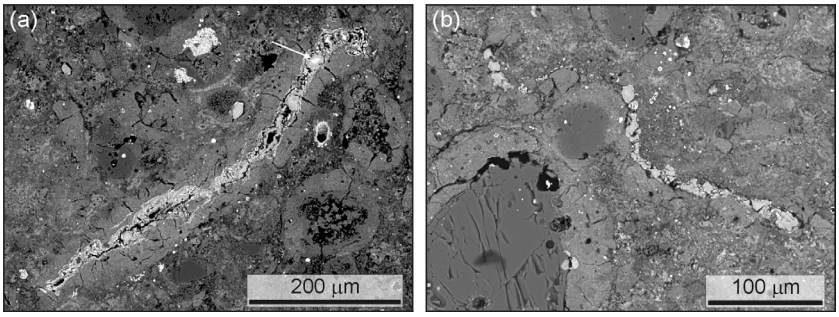


Fig. 11. BSE images of Fe-rich veins in LEW 85311,31. (a) A vein enclosed within a narrow FGR. Most of the vein is close in chemical composition to tochilinite. Relict kamacite (white) is indicated by an arrow. (b) A vein composed mainly of tochilinite and P-rich sulphide. It wraps around a small chondrule fragment in a manner suggesting that its enclosing matrix has undergone ductile deformation.

The size distribution of LEW 85311 chondrules and chondrule fragments can potentially provide valuable information about this meteorite's relationship to carbonaceous chondrite groups. For example, chondrules in CV and CK meteorites have a larger apparent diameter than those in COs and CMs (Friedrich et al., 2015). However, the only data on CM chondrule sizes that was available to Friedrich et al. (2015) was an analysis of 100 chondrules in Murray, which have an average apparent diameter of 270 ± 240 μm (Rubin and Wasson, 1986). The size distribution of chondrules and chondrule fragments has recently been determined for Jbilet Winselwan (CM) (Friend et al., 2018). Two different lithologies were studied, whose chondrules and chondrule fragments were of a similar apparent

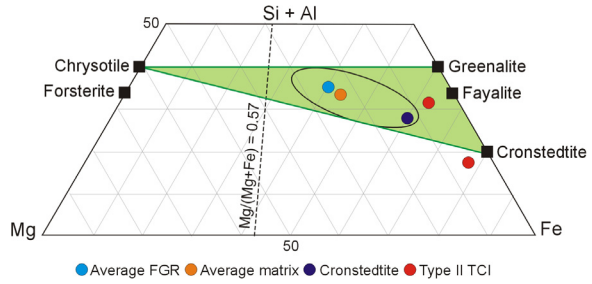


Fig. 12. Chemical composition of LEW 85311,39 matrix and FGRs (atomic %). The 92 analyses (21 matrix, 71 FGR) all plot within the oval area, and average matrix and FGR values are shown. Also plotted is an analysis of cronstedtite and two analyses of type II TCI from the LEW 85311 matrix (analysed by STEM-EDX), and the bulk Mg/(Mg + Fe) ratio of LEW 85311 (Si not measured). The serpentine field is coloured green, and black squares are stoichiometric mineral compositions. Individual analyses are provided in the supplementary data.

size (141 μm and 149 μm in the two lithologies). Friend et al. (2018) suggested that the difference between Jbilet Winselwan and Murray was because Rubin and Wasson (1986) did not measure chondrule fragments. The apparent diameter of LEW 85311 chondrules and chondrule fragments (213 ± 153 μm) falls between Jbilet Winselwan and Murray, and is much smaller than the CVs and CKs. In the absence of a larger dataset of the size of CM chondrules and chondrule fragments, the LEW 85311 measurements cannot be used to rigorously test the meteorite's relationship to the CMs. FGRs in LEW 85311 have an average apparent thickness of 37 μm, which is thinner than Jbilet Winselwan (59–76 μm) (Friend et al., 2018). However, the slope of the correlation between chondrule apparent diameter and FGR apparent thickness is similar between the two meteorites, implying comparable conditions of rim formation (LEW 85311 = 0.14; Jbilet Winselwan = 0.12–0.18) (Supplementary Fig. A3).

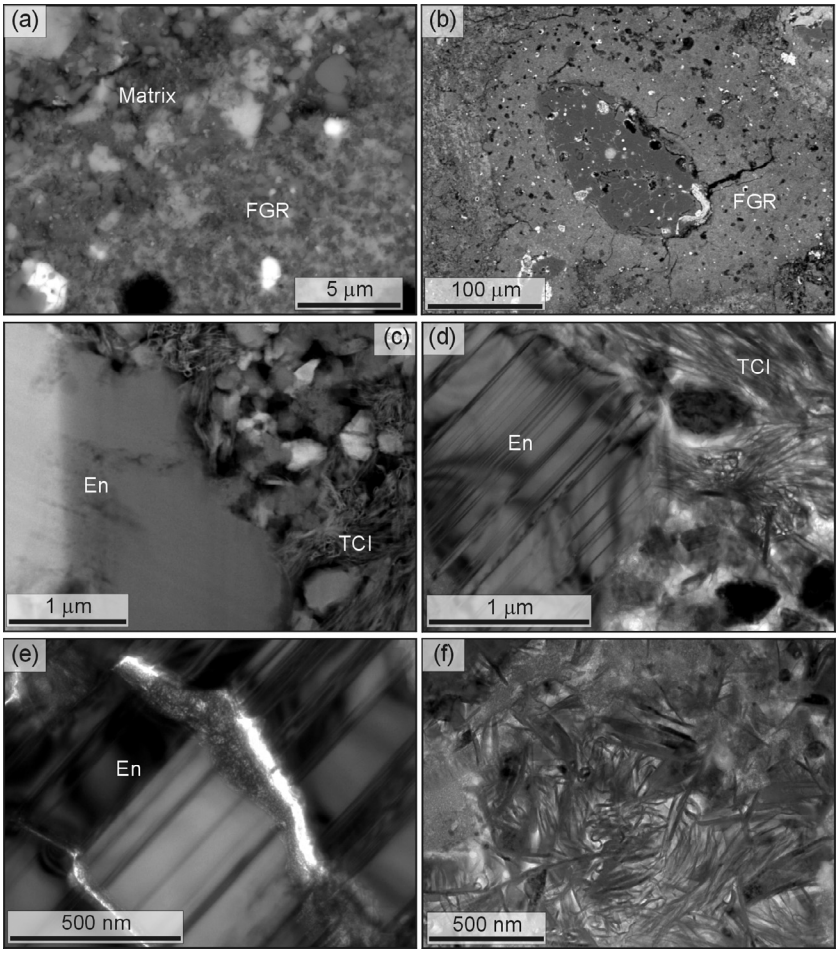


Fig. 13. Images of LEW 85311,39 FGRs. (a) BSE image of the contact between a FGR (lower right) and the enclosing matrix (upper left). The FGR contains grains of Fe-sulphide (white) and micropores (black). (b) BSE image of a type I chondrule that has a thick and micropore-rich FGR. (c) HAADF STEM image showing a relatively large and intact enstatite (En) crystal surrounded by grains of Fe-sulphide (white) and silicates (grey). Between these crystals are fine TCI fibres. (d) Bright-field TEM image of a similar field of view to (c) with an enstatite (En) grain surrounded by TCI fibres. (e) Interior of the enstatite (En) crystal in (c) and (d) showing a vein of poorly crystalline phyllosilicate. (f) Bright-field TEM image of a serpentine-rich area within a FGR.

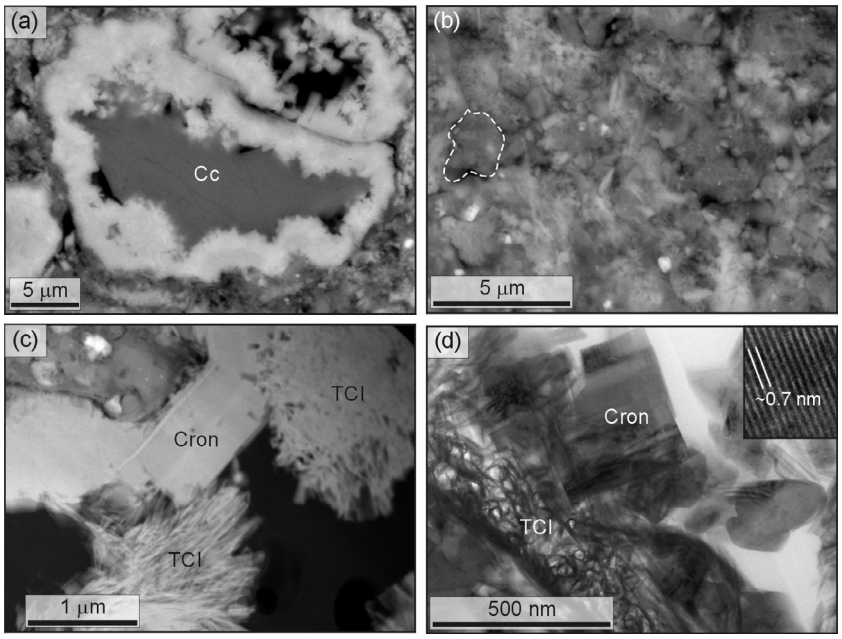


Fig. 14. Images of LEW 85311,39 matrix. (a) BSE image of a crystal of Ca-carbonate (Cc) that is rimmed by Fe-rich phyllosilicate (white). (b) BSE image of an area of matrix that contains ~1 μm size objects with a rounded/bulbous shape that are analogous to GEMS particles; one of them is delineated by a dashed white line. Micropores (black) occur between the objects. (c) HAADF STEM image showing a mass of type II TCI crystals and a platy cronstedtite (Cron) crystal. The black area is porosity. (d) Bright-field TEM image of a different part of the same sample as (c), again with an intimate intergrowth of type II TCI and cronstedtite. The inset high-resolution TEM image shows the lattice fringes of cronstedtite.

Table 9
Chemical composition (atomic %) of cronstedtite and type-II TCI in the matrix of LEW 85311,39 compared with cronstedtite and tochilinite in type-II TCI from Paris (CM).

| | LEW 85311 | | | Paris TCI | |
|---|---|---|---|---|---|
| | Cronstedtite | TCI | TCI | Cronstedtite[1] | Tochilinite[2] |
| Si | 9.1 ± 0.0 | 4.7 | 8.2 | 9.0 ± 0.8 | 1.0 ± 0.5 |
| Al | 0.9 ± 0.1 | 1.3 | 3.2 | 1.0 ± 0.4 | 0.5 ± 0.3 |
| Fe | 25.6 ± 0.7 | 26.4 | 23.5 | 21.3 ± 2.5 | 34.0 ± 2.5 |
| Ni | – | 0.9 | 0.4 | n.a. | n.a. |
| Mg | 1.1 ± 0.0 | 2.3 | 2.3 | 3.1 ± 1.5 | 2.3 ± 0.5 |
| S | – | 9.0 | 2.1 | n.a. | 19.3 ± 1.0 |
| O | 63.5 ± 0.9 | 55.4 | 60.3 | 65.6 ± 1.7 | 42.5 ± 2.6 |
| Total | 100.0 | 100.0 | 100.0 | 100.0 | 99.6 |
| n | 2 | 1 | 1 | 39 | 25 |

Analyses by TEM-EDX.
The two analyses of LEW 85311 TCI chosen to illustrate the compositional range.
n.a. – not analysed.
± One standard deviation.
Individual analyses for LEW 85311 provided in the supplementary data.
[1] Pignatelli et al. (2017, Table 3). Average of olivine- and pyroxene-hosted.
[2] Pignatelli et al. (2017, Table 2). Average of olivine- and pyroxene-hosted.

LEW 85311 refractory inclusions are similar in mineralogy to those that have been described from the CMs (Greenwood et al., 1994; Rubin, 2007). They are however smaller on average: 105 ± 88 μm in LEW 85311 versus 130 ± 90 μm (n = 40) and 130 ± 80 μm (n = 37) for the mildly altered CMs QUE 97,990 and Paris, respectively (Rubin, 2007, 2015). LEW 85311 refractory inclusions are considerably more abundant than in the other two CMs (146/cm$^2$ in LEW 85311 *vs* ~80/cm$^2$ in QUE 97990 and 34/cm$^2$ in Paris; Rubin, 2007, 2015). This high density of refractory inclusions is the most likely explanation for refractory element and REEs composition of LEW 85311, which falls between Paris and the CVs (Fig. 1). As refractory inclusions are $^{16}$O-rich, their unusually high concentra-

tion within LEW 85311 may also explain why its bulk oxygen isotopic composition plots within the CV-CO-CK field (Fig. 2). The difference between our analysis and the bulk measurement by Clayton and Mayeda (1999) may simply reflect intra-meteorite heterogeneity in the abundance of refractory inclusions. The low degree of aqueous alteration and commensurately low volume of matrix of LEW 85311 (Table 5) could also contribute to its bulk oxygen isotopic composition because the meteorite's fine grained matrix has a considerably higher $\delta^{17}O$ and $\delta^{18}O$ value than its chondrules and refractory inclusions (Clayton and Mayeda, 1999; Fig. 2). The close similarity in volatile element compositions between LEW 85311 and Paris shows that the two meteorites sample parent body regions that accreted a similar range of volatile-bearing components, and that the nature of any fractionation during subsequent parent body processing was also comparable.

#### 4.1.2. Agents of geological processing

By analogy with the CMs, post-accretionary processing of the LEW 85311 parent body could have included one or more of: (i) shock metamorphism; (ii) brecciation; (iii) aqueous alteration; (iv) post-hydration heating (Brearley, 2006). After falling to Earth the meteorite may also have been weathered (Lee and Bland, 2004). The S1 shock stage of LEW 85311 demonstrates that it has not experienced pressures of >4–5 GPa (Stöffler et al., 1991) so that its localized and mild petrofabric can be explained by compaction accompanying one or more low intensity impacts (e.g., Lindgren et al., 2015). None of the three thin sections contains clasts, thus showing that these impacts were sufficiently gentle that there was no brecciation or mixing (i.e., deformation was ductile). The intact crystal structures of tochilinite and serpentine constrain the intensity of heating that LEW 85311 could have experienced after aqueous alteration. Estimates of the temperature at which tochilinite breaks down range from 120 °C (Zolensky et al., 1997) to 300 °C (Tonui et al., 2014), and serpentine starts to degrade at ~300 °C (Akai, 1992). Kimura et al. (2011) used metal composition and sulphide texture to explore heating of the CMs. They placed LEW 85311 in their group "A", showing that it had not been significantly heated before/during aqueous alteration, which would have affected the Fe, Ni metal, or after aqueous alteration, which would have been identifiable by the presence of pentlandite lamellae/blebs in pyrrhotite. This lack of evidence for heating is also consistent with the unshocked and unbrecciated nature of LEW 85311 showing that it did not experience high impact temperatures. We therefore conclude that water-mediated alteration (parent body and/or terrestrial) was the main agent of post-accretionary processing of LEW 85311.

#### 4.1.3. Mechanisms and products of aqueous alteration

The principal evidence for aqueous alteration of LEW 85311 is the dissolution of some original components, and precipitation of new phases (i.e., phyllosilicates, sulphides, carbonates). Here we evaluate the nature of the geochemical reactions, the environments of water/rock interaction, and similarities to the CMs.

Dissolution of chondrule mesostasis glass has left pore spaces between phenocrysts, whereas the relatively large and rounded voids within chondrules may have formed by dissolution of Fe, Ni metal nuggets. The irregular/-faceted pores within FGRs were most likely produced by dissolution of one or more primary minerals (e.g., fayalitic olivine, metal, sulphide), and the greater abundance of these pores in outer parts of the rims may indicate that fluids responsible were hosted in the matrix. There is no evidence to determine the environment of chondrule and FGR dissolution (i.e., parent body, terrestrial or both).

Serpentine, cronstedtite, tochilinite and TCI were identified by XRD and TEM, and are characteristic products of CM parent body aqueous alteration (Bunch and Chang, 1980; Barber, 1981; Mackinnon and Zolensky, 1984; Tomeoka and Buseck, 1985). Where they occur in the matrix and FGRs, these minerals are assumed to have formed at the expense of fine-grained silicate, sulphide and metal, and probably also ~1 μm size GEMS-like particles. The absence of large TCI clumps distinguishes LEW 85311 from the moderately to highly altered CMs (they comprise 15–40 vol.% of CM2.2–2.6 meteorites (Rubin et al., 2007; Rubin 2015)). Evidence for replacement of coarser grained silicates by phyllosilicates is restricted to occasional grains of fayalitic olivine and one crystal of gehlenite. By contrast, nuggets and veins of kamacite have been extensively replaced by tochilinite, P-rich sulphide and schreibersite. Alteration of kamacite to sulphides was a common reaction during the initial stages of aqueous processing of the CMs within geochemical environments with a high S activity (Tomeoka and Buseck, 1985; Palmer and Lauretta, 2011). Overall, the processes and products of aqueous alteration of LEW 85311 are closely comparable to 'Stage 1′ of the four-stage CM aqueous alteration sequence that was described by Hanowski and Brearley (2001) and refined by Velbel et al. (2012). Thus the geochemical environment within the LEW 85311 parent body was similar to the mildly altered CMs (i.e., pH, Eh, water/rock ratio, temperature).

By analogy with Antarctic ordinary chondrites (Buchwald and Clarke, 1989; Lee and Bland, 2004), the akaganéite-bearing mantles to kamacite grains are interpreted to have formed by terrestrial weathering. Thus, LEW 85311 has been modified by reaction with water both pre- and post-terrestrially, a combination of processes that is common to the CM Elephant Moraine (EET) 96029 (Lee et al., 2016), and probably many other Antarctic carbonaceous chondrites.

*4.1.3.1. Ca-carbonate.* Ca-carbonate is rare in LEW 85311. It was not detected by XRD, and Alexander et al. (2015) recorded 0.3 wt.% carbonate-hosted carbon in bulk samples of both LEW 85311 and LEW 85312; this value is lower than 42 of the 43 unheated CMs analysed by Alexander et al. (2015). Ca-carbonate occurs in three contexts: (i) within a gehlenite-bearing refractory inclusion (Fig. 8d); (ii) scarce small crystals within the matrix (Fig. 14a); (iii) meshworks of needle-fibre calcite (Figs. 9 and 10). By analogy with calcite in refractory inclusions from the CM falls Murchison (Armstrong et al., 1982) and Murray (Lee and

Greenwood, 1994), Ca-carbonate in the LEW 85311 refractory inclusion is interpreted to have formed by parent body aqueous alteration. This conclusion is consistent with experimental results showing that gehlenite alters to calcite when it reacts with carbonate-rich solutions under hydrothermal conditions (Nomura and Miyamoto, 1998). As the matrix-hosted Ca-carbonate has been partially replaced by phyllosilicates, in common with calcite in the matrices of CM falls (Lee et al., 2014), it is likewise interpreted to be the product of parent body processing.

Needle-fibre calcite could have formed on the parent body or by terrestrial weathering, and these two environments can be distinguished using its C and O isotopic composition. Given that the needle-fibre calcite is by far the most abundant type of Ca-carbonate in each of the three LEW 85311 thin sections, its isotopic composition should be close to that of bulk Ca-carbonate in LEW 85311 ($\delta^{18}O$ 19.4 ± 0.9‰, $\delta^{13}C$ 28.6 ± 0.2‰) and LEW 85312 ($\delta^{18}O$ 23.0 ± 0.3‰, $\delta^{13}C$ 34.1 ± 0.2‰) (Alexander et al., 2015). In Supplementary Fig. A4 these values are plotted along with the 43 CMs in Alexander et al. (2015), terrestrial calcite in an Antarctic CM ($\delta^{18}O$ −9‰, $\delta^{13}C$ ~0‰; Tyra et al., 2007), and terrestrial Ca-carbonate from Antarctic ordinary chondrites ($\delta^{18}O$ 3–30‰, $\delta^{13}C$ = ~6‰; Evans et al., 2017). The carbon isotopic composition of bulk LEW 85311 and LEW 85312 Ca-carbonate is very different to the Antarctic weathering products, and so the needle-fibre calcite is interpreted to have formed on the LEW 85311 parent body. The LEW 85311 and 85312 data plot towards the low $\delta^{13}C$ and $\delta^{18}O$ end of the trend defined by the CMs in Supplementary Fig. A4. Alexander et al. (2015) interpreted this trend to reflect differences in temperature of the carbonate-precipitating fluids (ranging from ~0 to 130 °C), thus implying that LEW 85311 and LEW 85312 Ca-carbonate would have formed in the higher temperature part of the range.

Despite being isotopically consistent with the CMs, LEW 85311 needle-fibre calcite is distinct in its petrographic context, and crystal size and shape. CM calcite occurs most commonly in the matrix as relatively coarse and equant grains, suggestive of slow rates of crystal growth from fluids of a low degree of supersaturation (Johnson and Prinz, 1993; de Leuw et al., 2010; Lee et al., 2014). Conversely, the small size of the needle-fibre crystals and their random orientations relative to each other imply rapid crystal growth from highly supersaturated solutions. Terrestrial calcite that is very similar in crystal size and shape is termed 'moonmilk'; it occurs in caves and burial tombs and forms by evaporation (Cirigliano et al., 2018; Spotl, 2018; Lee et al., 2019a,b). We therefore propose that LEW 85311 needle-fibre calcite is also a parent body evaporite. The consistent association of needle-fibre calcite with kamacite and its alteration products (P-rich sulphide, Fe-sulphide, schreibersite, tochilinite, eskolaite) suggests that the metal was aqueously altered prior to carbonate precipitation, making space for the calcite. These kamacite grains must have been relatively large (up to several hundred micrometres in diameter) and free-floating in the solar nebular so that they accreted FGRs (Hanna and Ketcham, 2018). Most of the calcite-rich objects are rounded (Fig. 10), but several have a shard-like shape (Fig. 9e) suggestive of brittle breakage of kamacite prior to accretion of the FGR. The geochemical conditions under which kamacite alteration would associate with calcite precipitation are unknown. However, the common intergrowth of calcite with TCI in CM matrices (Tomeoka and Buseck, 1985; Lee et al., 2014) is evidence for a genetic link between carbonate and sulphide precipitation in carbonaceous chondrite parent bodies.

### 4.2. Degree of aqueous alteration

LEW 85311 has been mildly altered when assessed relative to the mineralogical and geochemical criteria that are used for the CMs. Kimura et al. (2011) found that it has a "low" degree of aqueous alteration. LEW 85311 and its pair LEW 85312 have been assigned to petrologic types of 1.9/1.8 (Alexander et al., 2013) and 1.7 (from XRD data in Table 4) (Table 1). Relative to the petrologic subtypes of Rubin et al. (2007), LEW has been tentatively assigned to CM2.6–2.7 (Choe et al., 2010) and to CM2.3 (Friedrich et al., 2018). These two different subtype assignments can be tested by comparison with the petrologic types of LEW 85311. There is a good linear correlation between the three classification schemes for meteorites of petrologic subtypes 2.0–2.6. (Supplementary Fig. A5). However, as there are no meteorites have been classified at CM2.7 or higher on the Rubin et al. (2007) scheme that have also been measured by Alexander et al. (2013) or Howard et al. (2015), the nature of the correlation lines at lower degrees of aqueous alteration cannot be determined. Nonetheless, as a petrologic subtype of 3.0 on the Rubin et al. (2007) scale should equal a petrologic type of 3.0 on the other two scales, the regression lines in Supplementary Fig. A5 can be extrapolated between CM2.6 and CM3.0. Using these lines, a petrologic type of 1.9–1.8 corresponds to ~CM2.7–CM2.6, and 1.7 corresponds to ~CM2.6 (Supplementary Fig. A5). Taking the two comparisons together suggests a subtype of CM2.7–CM2.6 for LEW 85311, in agreement with Choe et al. (2010).

It is difficult to assign LEW 85311 to a petrologic subtype directly because the meteorite lacks large "PCP clumps", whose abundance and chemical composition are key metrics in the Rubin et al. (2007) scheme. The other criteria of Rubin et al. (2007) are consistent with a subtype of CM2.6 or higher for LEW 85311 apart for the abundance of Fe, Ni metal. They propose that meteorites of subtype CM2.5 and CM2.6 should contain 0.03–0.3 vol.% and ~1 vol.% metallic Fe-Ni, respectively. As XRD shows that LEW 85311 contains 0.3 vol.% metal, a ~CM2.5 classification is suggested. However, the only meteorite classified by Rubin et al. (2007) as CM2.6 was QUE 97990, which contains 0.2 vol.% Fe,Ni metal as quantified by XRD (Howard et al. 2015). Furthermore, the 0.3 vol.% Fe,Ni metal is equal to its abundance in EET 96029 (a heated CM2.7; Lee et al., 2016), and only one of the 36 CMs plotted in Fig. 3 is richer in metal. Therefore by using XRD-determined metal abundance alone, LEW 85311 is less altered than QUE 97,990 and so should be assigned to a subtype of CM2.6 or higher. The lack of chondrule glass

that is preserved in EET 96029 (CM2.7) and Paris (CM2.7; Marrocchi et al., 2014, Rubin 2015) argues against LEW 85311 being significantly more pristine than these two CMs, and so we conclude overall that it has a petrologic subtype of CM2.7.

A variety of other properties of LEW 85311 are comparable to those of the most weakly aqueously altered CMs, which further demonstrates that LEW 85311 evolved in a comparable manner. Mild alteration is consistent with the preservation of gehlenite, which is highly reactive in the presence of liquid water (e.g., Rubin, 2007). LEW 85311 has a low phyllosilicate fraction (Table 4), showing that alteration stopped early (i.e., Stage 1 of Hanowski and Brearley, 2001) thereby preserving much of the original olivine and pyroxene. XRD also shows a high ratio of cronstedtite to Mg,Fe serpentine. Little of the early formed cronstedtite had recrystallized to Mg-serpentine because the main sources of magnesium needed for this reaction are Mg-rich olivine and pyroxene, which are more resistant to parent body aqueous alteration than their Fe-rich equivalents (Tomeoka and Buseck, 1985; Tomeoka et al., 1989; Howard et al., 2009). The Mg/(Mg + Fe) of tochilinite after kamacite in LEW 85311 is lower than the mildly altered CMs Murchison and Murray (Table 7), again because relatively little Mg had been liberated from Mg-rich olivine and pyroxene that would otherwise have been available to increase its Mg/(Mg + Fe) (Palmer and Lauretta, 2011). This limited supply of Mg during aqueous alteration is also expressed by the MgO/FeO value of LEW 85311 matrix (0.33), which is significantly lower than that of Paris (0.39) (Supplementary Table A3). Finally, data in Nazarov et al. (2009) show a relationship between the chemical composition of P-rich sulphides and degree of aqueous alteration of their host meteorite, and accordingly LEW 85311 P-rich sulphides have a composition similar to those in the most mildly altered CMs (Table 8). Therefore, multiple proxies agree that LEW 85311 has been mildly altered, and its geochemical and mineralogical evolution followed a trajectory closely comparable to the most weakly hydrated CMs.

### 4.3. Affinity of LEW 85311

This meteorite has many similarities to the CMs, but also some important differences that have prompted us to question its link to the group. The CMs are homogeneous in chemical composition (Rubin et al., 2007; Braukmüller et al., 2018; Friedrich et al., 2018), with any small differences between meteorites being potentially attributable to terrestrial weathering (Friedrich et al., 2018). This compositional homogeneity has been interpreted to demonstrate that the CM3 starting material was chemically uniform and aqueous alteration was isochemical (i.e., closed aqueous system) so that water-soluble elements (e.g., Na, K) were not leached (e.g., Brearley, 2006; Rubin et al., 2007; Bland et al., 2009; Velbel et al., 2012; Braukmüller et al., 2018; Friedrich et al., 2018). Rubin et al. (2007) concluded that the compositional homogeneity of the CMs indicates a single parent body for the group.

LEW 85311 sits outside of the narrow range of CM chemical compositions (i.e., principally in its refractory elements and REEs; Fig. 1). We contend that this divergence from the CMs is due to a different starting material (i.e., one rich in refractory inclusions) that was isochemically altered. An alternative explanation is that this meteorite was initially chemically similar to other CMs but changed in composition during open system aqueous alteration. However, in such a scenario LEW 85311 would be expected to differ from the CMs in its water-soluble elements rather than the most highly refractory elements as is observed (Fig. 1). Moreover, Mg should have been selectively leached, yet the chemical compositions of Mg-bearing alteration products (e.g., matrix and FGR phyllosilicates and tochilinite) are consistent with mildly altered CMs. The oxygen isotopic compositions of the CMs are quite variable, in part due to contrasting degrees of aqueous alteration and in a few cases also post-hydration heating (Clayton and Mayeda, 1999). LEW 85311 falls outside of the CM range (Fig. 2), but its unusual isotope values can again be explained by abundant refractory inclusions.

LEW 85311 is almost indistinguishable from the mildly altered CMs with regards to the processes and products of aqueous alteration (i.e., alteration of kamacite, sulphide, amorphous silicates and the most reactive silicate minerals to cronstedtite, serpentine and sulphides). These alteration products also include tochilinite, which is a mineralogical 'hallmark' of the CMs. The only evidence for a difference in alteration between LEW 85311 and the CMs is the presence of needle-fibre calcite, which may have formed by evaporation of relatively high temperature parent body fluids, and the absence from the matrix of TCI 'clumps'. Despite these differences, LEW 85311 is interpreted to have originally contained a similar proportion of water ice to many of the CMs, then was heated and remained warm for a sufficient length of time to be mildly aqueously altered.

NWA 5958 is a hydrated carbonaceous chondrite with some similarities to LEW 85311. It has been classified as C2-ung and its bulk oxygen isotopic composition plots within the CV-CO-CK field close to one of the analyses of LEW 85311 (Jacquet et al., 2016) (Fig. 2). However there is no petrographic or geochemical evidence for an elevated abundance of refractory inclusions that could otherwise account for this $^{16}$O-rich composition (Ash et al., 2011; Jacquet et al., 2016). Jacquet et al. (2016) found that NWA 5958 is moderately aqueous altered relative to the CMs (~CM2.5 subtype), and its infra-red spectrum closely resembles that of LEW 85311, especially in the 10 μm region. The similarities between NWA 5958 and LEW 85311 require further investigation, and one intriguing suggestion is that along with other 'anomalous' meteorites, NWA 5958 and LEW 85311 may be members of a new group of 'primitive' carbonaceous chondrites with CM affinities (Greenwood et al., 2019).

We set out to ask whether LEW 85311 can provide new insights into the diversity of hydrated C-complex meteorite parent bodies. Our work has shown that the material accreted to form LEW 85311 was subtly different to the CMs, particularly with regards to the abundance of refractory inclusions, yet this meteorite's subsequent mineralogical and geochemical evolution was very similar to other

members of the group. We therefore conclude that the CM classification is appropriate, and that the diversity within the group shows that the CMs sample two or more parent bodies that accreted in a similar part of the solar nebula, and grew to a comparable size and at over a common timescale (thus possessing a similar complement of short-lived radiogenic isotopes) so that they had an equivalent geological evolution. We anticipate that the forthcoming return of samples from the 'rubble pile' asteroids Ryugu (Watanabe et al., 2019) and Bennu (Lauretta et al., 2019) will greatly enhance our understanding of the nature and diversity of C-complex asteroids.

## 5. CONCLUSIONS

LEW 85311 is a CM carbonaceous chondrite, and most of its properties are consistent with other members of the group. It is composed of rimmed chondrules, chondrule fragments and refractory inclusions supported within a fine-grained matrix. The chondrules and chondrule fragments are similar in size to those of the CMs, although their FGRs are relatively thin. LEW 85311 has undergone parent body aqueous processing, and many of the alteration products (e.g., serpentine, cronstedtite, tochilinite, P-rich sulphide, TCI) are indistinguishable in mineralogy and chemical composition to those of the most mildly altered CMs. However, there is evidence for a distinctive geochemical environment during aqueous alteration of LEW 85311 from the presence of meshworks of needle-fibre calcite within objects that were previously rich in kamacite, and the absence of TCI clumps. LEW 85311 is comparable to the CMs in its volatile element composition, but differs in its refractory element, REE and bulk oxygen isotopic composition owing to a high abundance of refractory inclusions. It also accreted an unusually low proportion of water ice, which limited the degree of aqueous alteration. LEW 85311 shows that the CM group samples more than one parent body.

## ACKNOWLEDGEMENTS

We thank Peter Chung for help with the SEM work, and are grateful to ANSMET for providing the samples of LEW 85311. US Antarctic meteorite samples are recovered by the Antarctic Search for Meteorites (ANSMET) program, which has been funded by NSF and NASA, and characterized and curated by the Department of Mineral Sciences of the Smithsonian Institution and Astromaterials Acquisition and Curation Office at NASA Johnson Space Center. This work was funded by the UK Science and Technology Facilities Council through grant ST/N000846/1. Author contributions: M.R.L. and B. E. C. designed the research project; M.R.L., B.E.C., A.J.K. and R.C.G. undertook analyses and contributed to writing and editing of the manuscript; M.R.L. acquired funding. We thank Alan Rubin and an anonymous reviewer for their helpful comments on the manuscript.

## APPENDIX A. SUPPLEMENTARY MATERIAL

Supplementary data to this article can be found online at https://doi.org/10.1016/j.gca.2019.07.027.

## REFERENCES

Akai J. (1992) T-T–T diagram of serpentine and saponite, and estimation of metamorphic degree of Antarctic carbonaceous chondrites. *Proc. Nat. Inst. Polar Res. Symp. Antarctic Meteorit.* **5**, 120–135.

Alexander C. M. O'D., Bowden R., Fogel M. L., Howard K. T., Herd C. D. K. and Nittler L. R. (2012) The provenances of asteroids, and their contributions to the volatile inventories of the terrestrial planets. *Science* **337**, 721–723.

Alexander C. M. O'. D., Howard K. T., Bowden R. and Fogel M. L. (2013) The classification of CM and CR chondrites using bulk H, C and N abundances and isotopic compositions. *Geochim. Cosmochim. Acta* **123**, 244–260.

Alexander C. M. O'. D., Bowden R., Fogel M. L. and Howard K. T. (2015) Carbonate abundances and isotopic compositions in chondrites. *Meteorit. Planet. Sci.* **50**, 810–833.

Alexander C. M. O'. D., Greenwood R. C., Bowden R., Gibson J. M., Howard K. T. and Franchi I. A. (2018) A multi-technique search for the most primitive CO chondrites. *Geochim. Cosmochim. Acta* **221**, 406–420.

Armstrong J. T., Meeker G. P., Huneke J. C. and Wasserburg G. J. (1982) The Blue Angel: I. the mineralogy and petrogenesis of a hibonite inclusion from the Murchison meteorite. *Geochim. Cosmochim. Acta* **46**, 575–595.

Ash R. D., Walker R. J., Puchtel I. S., McDonough W. F. and Irving A. J. (2011) The trace element chemistry of Northwest Africa 5958, a curious primitive carbonaceous chondrite (abstract #2325). *42nd Lunar and Planetary Science Conference*.

Barber D. J. (1981) Matrix phyllosilicates and associated minerals in C2M carbonaceous *chondrites*. *Geochim. Cosmochim. Acta* **45**, 945–970.

Bland P. A., Jackson M. D., Coker R. F., Cohen B. A., Webber J. B. W., Lee M. R., Duffy C. M., Chater R. J., Ardakani M. G., McPhail D. S., McComb D. W. and Benedix G. K. (2009) Why aqueous alteration in asteroids was isochemical: high porosity ≠ high permeability. *Earth Planet. Sci. Lett.* **287**, 559–568.

Braukmüller N., Wombacher F., Hezel Dominik C., Escoube R. and Münker C. (2018) The chemical composition of carbonaceous chondrites: Implications for volatile element depletion, complementarity and alteration. *Geochim. Cosmochim. Acta* **239**, 17–48.

Brearley A. J. (2006) The action of water. In *Meteorites and the Early Solar System II* (eds. D. S. Lauretta, H. Y. McSween, D. S. Lauretta and H. Y. McSween). University of Arizona Press, pp. 587–624.

Buchwald V. F. and Clarke Jr R. S. (1989) Corrosion of Fe-Ni alloys by Cl-containing akaganèite (β-FeOOH): The Antarctic meteorite case. *Am. Mineral.* **74**, 656–667.

Bunch T. E. and Chang S. (1980) Carbonaceous chondrites – II. Carbonaceous chondrite phyllosilicates and light element geochemistry as indicators of parent body processes and surface conditions. *Geochim. Cosmochim. Acta* **44**, 1543–1577.

Burbine T. H. (2017) Asteroids: Astronomical and Geological Bodies. Cambridge University Press, 367 pp.

Chizmadia L. J. and Brearley A. J. (2008) Mineralogy, aqueous alteration, and primitive textural characteristics of fine-grained rims in the Y-791198 CMS carbonaceous chondrite: TEM observations and comparison to ALHA81002. *Geochim. Cosmochim. Acta* **72**, 602–625.

Choe W. H., Huber H., Rubin A. E., Kallemeyn G. W. and Wasson J. T. (2010) Compositions and taxonomy of 15 unusual carbonaceous chondrites. *Meteorit. Planet. Sci.* **45**, 531–554.

Cirigliano A., Tomassetti M. C., Di Pietro M., Mura F., Maneschi M. L., Gentili M. D., Cardazzo B., Arrighi C., Mazzoni C., Negri R. and Rinaldi T. (2018) Calcite moonmilk of microbial

origin in the Etruscan Tomba degli Scudi in Tarquinia, Italy. *Sci. Rep.* **8**, 15839.

Clayton R. N. and Mayeda T. K. (1999) Oxygen isotope studies of carbonaceous chondrites. *Geochim. Cosmochim. Acta* **63**, 2089–2104.

Cloutis E. A., Hudon P., Hiroi T., Gaffey M. J. and Mann P. (2011) Spectral reflectance properties of carbonaceous chondrites: 2. CM chondrites. *Icarus* **216**, 309–346.

de Leuw S., Rubin A. E., Schmidt A. K. and Wasson J. T. (2010) Carbonates in CM chondrites: complex formational histories and comparison to carbonates in CI chondrites. *Meteorit. Planet. Sci.* **45**, 513–530.

DeMeo F. E., Binzel R. P., Slivan S. M. and Bus S. J. (2009) An extension of the Bus asteroid taxonomy into the near-infrared. *Icarus* **202**, 160–180.

Evans M. E., Niles P. B., Locke D. R. and Chapman P. (2017) Isotopic composition of carbonates in Antarctic ordinary chondrites and Miller Range nakhlites: Insights into Martian Amazonian aqueous alteration. *Lunar Planet. Sci.*, L#2727, (abstr.).

Friedrich J. M., Abreu N. M., Wolf S. F., Troiano J. M. and Stanek G. L. (2018) Redox-influenced trace element compositional differences among variably aqueously altered CM chondrites. *Geochim. Cosmochim. Acta* **237**, 1–17.

Friedrich J. M., Weisberg Michael K., Ebel Denton S., Biltz A. E., Corbett B. M., Iotzov I. V., Khan W. S. and Wolman M. D. (2015) Chondrule size and related physical properties: a compilation and evaluation of current data across all meteorite groups. *Chem. Erde* **75**, 419–443.

Friend P., Hezel D. C., Barrat J.-A., Zipfel J., Palme H. and Metzler K. (2018) Composition, petrology, and chondrule-matrix complementarity of the recently discovered Jbilet Winselwan CM2 chondrite. *Meteorit. Planet. Sci.* **53**, 2470–2491.

Greenwood R. C., Lee M. R., Hutchison R. and Barber D. J. (1994) Formation and alteration of CAIs in Cold Bokkeveld (CM2). *Geochim. Cosmochim. Acta* **58**, 1913–1935.

Greenwood R. C., Burbine T. H. and Franchi I. A. (2019) Linking asteroids and meteorites to the primordial parent body population: an oxygen isotope perspective. *Geochim. Cosmochim. Acta* (in review).

Greenwood R. C., Franchi I. A., Kearsley A. T. and Alard O. (2010) The relationship between CK and CV chondrites. *Geochim. Cosmochim. Acta* **74**, 1684–1705.

Greenwood R. C., Burbine T. H., Miller M. F. and Franchi I. A. (2017) Melting and differentiation of early-formed asteroids: the perspective from high precision oxygen isotope studies. *Chemie der Erde – Geochem.* **77**, 1–43.

Grossman J. N. (1994) The Meteoritical Bulletin, no. 76, 1994 January: The U.S. Antarctic Meteorite Collection. *Meteoritics* **29**, 100–143.

Hamilton V. E., Simon A. A., Christensen P. R., Reuter D. C., Clark B. E., Barucci M. A., Bowles N. E., Boynton W. V., Brucato J. R., Cloutis E. A., Connolly H. C., Donaldson Hanna K. L., Emery J. P., Enos H. L., Fornasier S., Haberle C. W., Hanna R. D., Howell E. S., Kaplan H. H., Keller L. P., Lantz C., Li J.-Y., Lim L. F., McCoy T. J., Merlin F., Nolan M. C., Praet A., Rozitis B., Sandford S. A., Schrader D. L., Thomas C. A., Zou X.-D. and Lauretta D. S. (2019) OSIRIS-REx Team Evidence for widespread hydrated minerals on asteroid (101955) Bennu. *Nat. Astron* **3**, 332–340.

Hanna R. D., Ketcham R. A., Zolensky M. and Behr W. M. (2015) Impact-induced brittle deformation, porosity loss, and aqueous alteration in the Murchison CM chondrite. *Geochim. Cosmochim. Acta* **171**, 256–282.

Hanna R. D. and Ketcham R. A. (2018) Evidence for accretion of fine-grained rims in a turbulent nebula for CM Murchison. *Earth Planet Sci Lett.* **481**, 201–211.

Hanowski N. P. and Brearley A. J. (2001) Aqueous alteration of chondrules in the CM carbonaceous chondrite, Allan Hills 81002: Implications for parent body alteration. *Geochim. Cosmochim. Acta* **65**, 495–518.

Hewins R. H., Bourot-Denise M., Zanda B., Leroux H., Barrat J.-A., Humayun M., Göpel C., Greenwood R. C., Franchi I. A., Pont S., Lorand J.-P., Courne'de C., Gattacceca J., Rochette P., Kuga M., Marrocchi Y. and Marty B. (2014) The Paris meteorite, the least altered CM chondrite so far. *Geochim. Cosmochim. Acta* **124**, 190–222.

Howard K. T., Benedix G. K., Bland P. A. and Cressey G. (2009) Modal mineralogy of CM2 chondrites by X-ray diffraction (PSD-XRD). Part 1: total phyllosilicate abundance and the degree of aqueous alteration. *Geochim. Cosmochim. Acta* **73**, 4576–4589.

Howard K. T., Benedix G. K., Bland P. A. and Cressey G. (2011) Modal mineralogy of CM chondrites by X-ray diffraction (PSD-XRD). Part 2: degree, nature and settings of aqueous alteration. *Geochim. Cosmochim. Acta* **75**, 2735–2751.

Howard K. T., Alexander C. M., D. O'., Schrader D. L. and Dyl K. A. (2015) Classification of hydrous meteorites (CR, CM and C2 ungrouped) by phyllosilicate fraction: PSD-XRD modal mineralogy and planetesimal environments. *Geochim. Cosmochim. Acta* **149**, 206–222.

Jacquet E., Barrat J.-A., Beck P., Caste F., Gattacceca J., Sonzogni C. and Gounelle M. (2016) Northwest Africa 5958: A weakly altered CM-related ungrouped chondrite, not a CI3. *Meteorit. Planet. Sci.* **51**, 851–869.

Johnson C. A. and Prinz M. (1993) Carbonate compositions in CM and CI chondrites, and implications for aqueous alteration. *Geochim. Cosmochim. Acta* **57**, 2843–2852.

Kallemeyn G. W. and Wasson J. T. (1981) The compositional classification of chondrites—I, the carbonaceous chondrite groups. *Geochim. Cosmochim. Acta* **45**, 1217–1230.

Kimura M., Grossman J. N. and Weisberg M. K. (2011) Fe-Ni metal and sulfide minerals in CM chondrites: An indicator for thermal history. *Meteorit. Planet. Sci.* **46**, 431–442.

King A. J., Schofield P. F. and Russell S. S. (2017) Type 1 aqueous alteration in CM carbonaceous chondrites: implications for the evolution of water-rich asteroids. *Meteorit. Planet. Sci.* **52**, 1197–1215.

King A. J., Russell S. S., Schofield P. F., Humphreys-Williams E. R., Strekopytov S., Abernathy F. A. J., Verchovsky A. B. and Grady M. M. (2019) The alteration history of the Jbilet Winselwan CM carbonaceous chondrite: an analogue for C-type asteroid sample return. *Meteorit. Planet. Sci.* **54**, 521–543.

Kitazato K. et al. (2019) The surface composition of asteroid 162173 Ryugu from Hayabusa2 near-infrared spectroscopy. *Science* **364**, 272–275.

Lauretta D. S. et al. (2019) The unexpected surface of asteroid (101955) Bennu. *Nature* **568**, 55–60.

Lee M. R. (1993) The petrography, mineralogy and origins of calcium sulphate within the Cold Bokkeveld CM carbonaceous chondrite. *Meteoritics* **28**, 53–62.

Lee M. R. and Greenwood R. C. (1994) Alteration of calcium- and aluminium-rich inclusions (CAIs) in the Murray (CM2) carbonaceous chondrite. *Meteoritics* **29**, 780–790.

Lee M. R., Lindgren P. and Sofe M. R. (2014) Aragonite, breunnerite, calcite and dolomite in the CM carbonaceous chondrites: high fidelity recorders of progressive parent body aqueous alteration. *Geochim. Cosmochim. Acta* **144**, 126–156.

Lee M. R., Lindgren P., King A. J., Greenwood R. C., Franchi I. A. and Sparkes R. (2016) Elephant Moraine 96029, a very

mildly aqueously altered and heated CM carbonaceous chondrite: implications for the drivers of parent body processing. *Geochim. Cosmochim. Acta* **92**, 148–169.

Lee M. R., Bland P. A. and Graham G. (2003) Preparation of TEM samples by focused ion beam (FIB) techniques: applications to the study of clays and phyllosilicates in meteorites. *Min. Mag.* **67**, 581–592.

Lee M. R. and Bland P. A. (2004) Mechanisms of weathering of meteorites recovered from hot and cold deserts and the formation of phyllosilicates. *Geochim. Cosmochim. Acta* **68**, 893–916.

Lee M. R., Cohen B. E., King A. J., Greenwood R. C. and Gibson J. (2019a) Moonmilk in the carbonaceous chondrites. *Lunar Planet. Sci.* **L#1367** (abstr.).

Lee M.R., Cohen B.E. and King A.J. (2019b) Alkali-halogen metasomatism of Meteorite Hills 01075 (CM2) driven by shock heating: An analogue for Ryugu. 82nd Annual Meteoritical Society Meeting 6070.pdf.

Leroux H., Cuvillier P., Zanda B. and Hewins R. H. (2015) GEMS-like material in the matrix of the Paris meteorite and the early stages of alteration of CM chondrites. *Geochim. Cosmochim. Acta* **170**, 247–265.

Lindgren P., Hanna R. D., Dobson K. J., Tomkinson T. and Lee M. R. (2015) The paradox between low shock-stage and evidence for compaction in CM carbonaceous chondrites explained by multiple low-intensity impacts. *Geochim. Cosmochim. Acta* **148**, 159–178.

Lodders K. (2003) Solar system abundances and condensation temperatures of the elements. *Astrophys. J.* **591**, 1220–1247.

Mackinnon I. D. R. and Zolensky M. E. (1984) Proposed structures for poorly characterized phases in C2M carbonaceous chondrite meteorites. *Nature* **309**, 240–242.

Mahan B., Moynier F., Beck P., Pringle E. A. and Siebert J. (2018) A history of violence: Insights into post-accretionary heating in carbonaceous chondrites from volatile element abundances, Zn isotopes and water contents. *Geochim. Cosmochim. Acta* **220**, 19–35.

Marrocchi Y., Gounelle M., Blanchard I., Caste F. and Kearsley A. T. (2014) The Paris meteorite: secondary minerals and asteroidal processing. *Meteorit. Planet. Sci.* **49**, 1232–1249.

McSween, Jr., H. Y. (1979a) Are carbonaceous chondrites primitive or processed? *Ann. Rev. Rev. Geophys. Space Phys.* **17**, 1059–1078.

McSween, Jr., H. Y. (1979b) Alteration in CM carbonaceous chondrites inferred from modal and chemical variations in matrix. *Geochim. Cosmochim. Acta* **43**, 1761–1770.

McSween, Jr., H. Y. (1987) Aqueous alteration in carbonaceous chondrites: Mass balance constraints on matrix mineralogy. *Geochim. Cosmochim. Acta* **51**, 2469–2477.

Metzler K., Bischoff A. and Stoffler D. (1992) Accretionary dust mantles in CM chondrites: evidence for solar nebula processes. *Geochim. Cosmochim. Acta* **56**, 2873–2897.

Miller M. F., Franchi I. F., Sexton A. S. and Pillinger C. T. (1999) High precision $\Delta^{17}O$ isotope measurements of oxygen from silicates and other oxides: methods and applications. *Rapid Commun. Mass Spectrom.* **13**, 1211–1217.

Nazarov M. A., Kurat G., Brandstaetter F., Ntaflos T., Chaussidon M. and Hoppe P. (2009) Phosphorus-bearing sulfides and their associations in CM chondrites. *Petrology* **17**, 101–123.

Nomura K. and Miyamoto M. (1998) Hydrothermal experiments on alteration of Ca-Al-rich inclusions (CAIs) in carbonaceous chondrites: implications for aqueous alteration in parent asteroids. *Geochim. Cosmochim. Acta* **62**, 3575–3588.

Palguta J., Schubert G. and Travis B. J. (2010) Fluid flow and chemical alteration in carbonaceous chondrite parent bodies. *Earth Planet. Sci. Lett.* **296**, 235–243.

Palmer E. E. and Lauretta D. S. (2011) Aqueous alteration of kamacite in CM chondrites. *Meteorit. Planet. Sci.* **46**, 1587–1607.

Pignatelli I., Marrocchi Y., Mugnaioli E., Bourdelle F. and Gounelle M. (2017) Mineralogical, crystallographic and redox features of the earliest stages of fluid alteration in CM chondrites. *Geochim. Cosmochim. Acta* **209**, 106–122.

Rubin A. E. (2007) Petrography of refractory inclusions in CM2.6 QUE 97990 and the origin of melilite-free spinal inclusions in CM chondrites. *Meteorit. Planet. Sci.* **42**, 1711–1729.

Rubin A. E. (2012) Collisional facilitation of aqueous alteration of CM and CV carbonaceous chondrites. *Geochim. Cosmochim. Acta* **90**, 181–194.

Rubin A. E. (2015) An American on Paris: extent of aqueous alteration of a CM chondrite and the petrography of its refractory and amoeboid olivine inclusions. *Meteorit. Planet. Sci.* **50**, 1595–1612.

Rubin A. E., Trigo-Rodriguez J. M., Huber H. and Wasson J. T. (2007) Progressive aqueous alteration of CM carbonaceous chondrites. *Geochim. Cosmochim. Acta* **71**, 2361–2382.

Rubin A. E. and Wasson J. T. (1986) Chondrules in the Murray CM2 meteorite and compositional differences between CM-CO and ordinary chondrite chondrules. *Geochim. Cosmochim. Acta* **50**, 307–315.

Schrader D. L., Davidson J., Greenwood R. C., Franchi I. A. and Gibson J. M. (2014) A water-ice rich minor body from the early Solar System: The CR chondrite parent body. *Earth Planet Sci. Lett.* **407**, 48–60.

Scott E. R. D., Keil K. and Stöffler D. (1992) Shock metamorphism of carbonaceous chondrites. *Geochim. Cosmochim. Acta* **56**, 4281–4293.

Sears D. W. G., Benoit P. H. and Jie L. (1993) Two chondrule groups each with distinc-tive rims in Murchison recognized by cathodoluminescence. *Meteoritics* **28**, 669–675.

Simon S. B., Keaton C. G. and Grossman L. (2005) Refractory inclusions from the CM2 chondrite LEW85311. *68th Annual Meteoritical Society Meeting (2005) 5122.pdf*.

Spötl C. (2018) Moonmilk as a human and veterinary medicine: evidence of past artisan mining in caves of the Austrian Alps. *Int. J. Speleol.* **47**, 127–135.

Starkey N. A., Jackson C. R. M., Greenwood R. C., Parman S., Franchi I. A., Jackson M., Fitton J. G., Stuart F. M., Kurz M. and Larsen L. M. (2016) Triple oxygen isotopic composition of high-$^{3}He/^{4}He$ mantle. *Geochim. Cosmochim. Acta* **176**, 227–238.

Stöffler D., Keil K. and Scott E. R. D. (1991) Shock metamorphism of ordinary chondrites. *Geochim. Cosmochim. Acta* **55**, 3845–3867.

Tomeoka K. and Buseck P. R. (1985) Indicators of aqueous alteration in CM carbonaceous chondrites: microtextures of a layered mineral containing Fe, S, O, and Ni. *Geochim. Cosmochim. Acta* **49**, 2149–2163.

Tomeoka K., McSween H. Y. and Buseck P. R. (1989) Mineralogical alteration of CM chondrites: a review. *Proc. Nat. Inst. Polar Res. Symp. Antarctic Meteorit.* **2**, 221–234.

Tonui E., Zolensky M., Hiroi T., Nakamura T., Lipschutz M., Wang M.-S. and Okudaira K. (2014) Petrographic, chemical and spectroscopic evidence for thermal metamorphism in carbonaceous chondrites I: CI and CM chondrites. *Geochim. Cosmochim. Acta* **126**, 284–306.

Trigo-Rodriguez J. M., Rubin A. E. and Wasson J. T. (2006) Non-nebular origin of dark mantles around chondrules and inclusions in CM chondrites. *Geochim. Cosmochim. Acta* **70**, 1271–1290.

Tyra M. A., Farquhar J., Wing B. A., Benedix G. K., Jull A. J. T., Jackson T. and Thiemens M. H. (2007) Terrestrial alteration of carbonate in a suite of Antarctic CM chondrites: evidence from oxygen and carbon isotopes. *Geochim. Cosmochim. Acta* **71**, 782–795.

Velbel M. A., Tonui E. K. and Zolensky M. E. (2012) Replacement of olivine by serpentine in the carbonaceous chondrite Nogoya (CM2). *Geochim Cosmochim. Acta* **87**, 117–135.

Watanabe S. et al. (2019) Hayabusa2 arrives at the carbonaceous asteroid 162173 Ryugu—a spinning top–shaped rubble pile. *Science* **364**, 268–272.

Weisberg M. K., McCoy T. J. and Krot A. N. (2006) Systematics and evaluation of meteorite classification. In *Meteorites and the Early Solar System II* (eds. D. S. Lauretta, H. Y. McSween, D. S. Lauretta and H. Y. McSween). University of Arizona Press, Arizona, USA, pp. 19–52.

Xiao X. and Lipschutz M. E. (1992) Labile trace elements in carbonaceous chondrites: a survey. *J. Geophys. Res. Planets* **97**, 10199–10211.

Zolensky M. E., Mittlefehldt D. W., Lipschutz M. E., Wang M.-S., Clayton R. N., Mayeda T. K., Grady M. M., Pillinger C. and Barber D. (1997) CM chondrites exhibit the complete petrologic range from type 2 to 1. *Geochim. Cosmochim. Acta* **61**, 5099–5115.

*Associate editor:* Christian Koeberl